QATAR UNIVERSITY

COLLEGE OF ARTS AND SCIENCES

Er DOPED GaN/AlN MULTIPLE QUANTUM WELL STRUCTURE FOR OPTOELECTRONIC DEVICES

BY

NUSYBA S. HASSAN

A Thesis Submitted to

the College of Arts and Sciences

in Partial Fulfillment of the Requirements for the Degree of

Masters of Science in Material Science and Technology

June 2021

© 2021 Nusyba S. Hassan. All Rights Reserved.

COMMITTEE PAGE

The members of the Committee approve the Thesis of

Nusyba S. Hassan defended on 25/04/2021.

Prof. Talal M. Altahtamouni

Thesis/Dissertation Supervisor

Dr Aboubakr M. Abdullah

Committee Member

Dr. Abdul Shakoor

Committee Member

Approved:

Ibrahim AlKaabi, Dean, College of Arts and Sciences

ABSTRACT

HASSAN, NUSYBA, S., Masters : June : [2021:], Material Science and Technology

Title: Er Doped GaN Quantum Well Structures for Optoelectronic Devices.

Supervisor of Thesis: Talal, M. Altahtamouni.

Rare-earth (RE) doped semiconductor materials have been widely investigated and studied for the exquisite properties they provide as dopants. Er is used to dope III-Nitrides mainly for its 1.54 µm emission, which is of high technological importance for applications in telecommunications, especially for fiber optics based communication. Epilayers of Er doped GaN (GaN:Er) and AlN (AlN:Er) have been successful in producing thermally stable emissions at 1.54 µm, however, the quantum efficiency of these Er doped epilayers is low to enable practical devices. Therefore, enhancement of the 1.54 µm emission intensity is needed. Using Er doped multiple quantum well (MQWs:Er) structures instead of Er doped epilayers was found to improve the quantum efficiency of the 1.54 µm through the improvement of the excitation of Er ions via the enhancement of the carrier density around Er ions. For that matter, we employed quantum well structures to host Er.

In this context, AlN/GaN:Er quantum well structures were synthesized by MOCVD on sapphire substrates. The structural, morphological and optical properties of the produced MQWs:Er were investigated by X-ray diffraction (XRD), time-of-flight secondary ion mass spectroscopy (ToF-SIMS) and Transmission electron microscopy (TEM), and Raman spectroscopy and it was shown that high quality MQWs were grown. The 1.54 µm emission properties of the MQWs were investigated by photoluminescence (PL) and the intensities of the 1.54 µm emission evaluated and

compared to Er doped GaN and Er doped AlN epilayers with a comparable Er doped active layer thickness. The comparison lead to the conclusion that the AlN/GaN:Er MQWs exhibited an enhanced PL intensity of more than 10 times that of the GaN:Er epilayer.

DEDICATION

"I dedicate this work to my great mother, my loving father and my supporting husband. Their continuous support and love made it possible."

ACKNOWLEDGMENTS

In the name of Allah, the almighty, all praise is due to Allah for his guidance and blessings which had led to the completion of this work.

I would like to extend my deep thanks and appreciation to my professor and thesis supervisor Prof. Talal Mohammed Al tahtamouni for his continuous support and motivation, help, guidance and for his understanding for the unforeseen conditions I was experiencing throughout the course of this work. My deep gratitude and acknowledgements are also extended to the committee members Dr. Aboubakr Abdullah and Dr. Abdul Shakoor. Also, many thanks to all the professors at the materials science and technology program for their effort throughout the master's classes, without which I wouldn't have the required knowledge and understanding to complete my degree. I would also like to express my deep thanks to the Core Labs at Qatar Energy and Environment Research institute for their help in executing STEM, and ToF-SIMS analyses and their constant willingness to help and support, thanks are especially extended to Dr Said Mansoor, director of Core Labs, and to Yahya Zakarya and Janarthanan Ponraj.

Finally, my sincere thanks for my family, friends and colleagues for their help, support and motivation.

TABLE OF CONTENTS

DEDICATION iv

ACKNOWLEDGMENTS v

LIST OF TABLES viii

LIST OF FIGURES ix

CHAPTER 1: INTRODUCTION 1

1.1 III-Nitride semiconductors 1

1.2 Aluminum Nitride (AlN) 6

1.3 Gallium Nitride (GaN) 8

CHAPTER 2: LITERATURE REVIEW 10

2.1 Rare-earth (RE) elements and RE doped semiconductors 10

2.2 Electronic configuration of Rare-Earth metals. 10

2.3 Excitation mechanisms of rare-earth doped III-Nitrides. 13

2.4 Erbium doped Semiconductors 15

2.5 Er-Doped AlN and GaN 18

2.6 Quantum Well structures 20

CHAPTER 3: EXPERIMENTAL METHODOLOGY 23

3.1 Synthesis technique: Metalorganic Chemical Vapor Deposition 23

CHARACTERIZATION TECHNIQUES 24

3.2 X-Ray Diffraction (XRD) 24

3.3 Raman spectroscopy 26

3.4 Time-of-Flight Secondary Ion Mass Spectroscopy (TOF-SIMS) 28

3.5 Scanning Transmission Electron Microscopy (STEM) 30

3.6 Photoluminescence Spectroscopy (PL) 32

CHAPTER 4: RESULTS AND DISCUSSION 35

4.1 MOCVD growth of AlN:Er , GaN:Er and AlN/GaN:Er MQW structure ... 35

4.2 Structural Properties 38

4.2.1 X-Ray Diffraction (XRD) 38

4.2.2 Raman spectroscopy 43

4.3 Transmission electron microscopy (TEM) 48

4.4 Surface Analysis: Time-of-Flight Secondary Ion mass spectroscopy (ToF-SIMS) 55

4.5 Optical properties: Photoluminescence spectroscopy. 56

CHAPTER 5: CONCLUSION 59

Future plans 60

REFERENCES 61

LIST OF TABLES

Table 1: Some chemical and physical properties of Aluminum Nitride (AlN). 7

Table 2: Chemical and physical properties of Gallium Nitride GaN............................9

Table 3: Electronic configuration of rare earth atoms and theri trivalent cations.....12

LIST OF FIGURES

Figure 1: Periodic table of the elements with highlighted group III-V and rare earth elements. 2

Figure 2: Band gap energies of III-Nitrides with their lattice parameters 2

Figure 3: An illustration of the difference between direct and indirect bandgap 4

Figure 4: Possible crystal structures of AlN and GaN 8

Figure 5: Dieke Diagram. 17

Figure 6: Effect of Temperature on the PL intensities of some Er doped semiconductors. 17

Figure 7: Visual representation of the structure of quantum wells. 21

Figure 8: Diagram of a CVD system 24

Figure 9: A schematic diagram of an XRD machine 25

Figure 10: visual representation of components of Bragg's law. 26

Figure 11: schematic diagram of a Raman spectrometer. 28

Figure 12: Thermo fisher scientific DXR Raman Microscope 28

Figure 13: Illustration of the surface analysis of ToF-SIMS 29

Figure 14: An illustration of a TEM (Left) and an example of a modern TEM instrument (right) [42]. 31

Figure 15: Image acquisition technique in TEM, Adapted from [43] 31

Figure 16: Principle of photoluminecence 33

Figure 17: A schematic diagram of a PL spectrophotometer 34

Figure 18: Maple II PL system. 34

Figure 19: Structure of AlN:Er (left) and GaN:Er (right) Epilayers 35

Figure 20: Growth temperature Vs growth time for the deposition of AlN:Er. 36

Figure 21: Growth temperature sequence of the Er doped AlN/GaN MQWs 37
Figure 22: layer structures of the Er Doped AlN/GaN MQWs 38
Figure 23: XRD patterns of GaN:Er epilayer. 39
Figure 24: XRD pattern of AlN:Er epilayer grown on sapphire. 40
Figure 25: XRD pattern of Er Doped AlN/GaN MQWs 41
Figure 26: Different phonons and their relative atomic displacements in Wz GaN with Ga atoms colored white [49],...44
Figure 27: Raman shifts of GaN:Er epilayer. 45
Figure 28: Raman shifts of AlN:Er epilayer. 46
Figure 29: Raman shifts of AlN/GaN:Er MQWs. 47
Figure 30: STEM images of MQWs:Er at different magnifications, bright strips are the GaN:Er Wells 49
Figure 31: Bright field STEM showing Interplanar spacing in the undoped AlN tempelate(a) and AlN/GaN:Er quantum wells (b) 50
Figure 32: SAED patterns for the undoped AlN buffer layer (Top) and the AlN/GaN:Er Quantum well structure (Bottom). 52
Figure 33: Energy dispersive spectroscopy elemental scanning of MQW:Er done using HAADF imaging. 54
Figure 34: ToF-SIMS profile of MQWs:Er showing Er^+, Ga^+ and Al^+ on a log scale y-axis. 56
Figure 35: PL spectrum of GaN:Er Epilayer 57
Figure 36: PL spectrum of AlN:Er epilayer 58
Figure 37: PL spectrum of AlN/GaN:Er MQWs. 58

CHAPTER 1: INTRODUCTION

In the recent years, the role of semiconductors has expanded rapidly in industry and consumer products, which has encouraged and fueled researchers to scavenge for newer, better performing and more reliable semiconductor materials. A very unique class of semiconductors are the III-Nitride compounds, III-Nitrides are a subcategory of the bigger family of III-V semiconductors formed by covalent bonding of an element from group III (e.g. B, Al, Ga, In) in the periodic table, with an element of group V (e.g. N, P, As, Sb). AlN, GaN, InN and their alloys (AlGaN, InGaN) are an important group of semiconductors used in optoelectronic devices due to their excellent performance as host materials for rare earth elements, owing this to their later discussed structural and optical properties.

1.1 III-Nitride semiconductors

The III-Nitrides are a distinguished class of semiconductors in both research and applicable industries, they started to gain the attention of scientific community more than 40 years ago [1][2]. Their applications are in a variety of devices used in one's daily life such as light emitting diodes (LED's) in televisions and mobile phones and also laser diodes (LD's) that made the high-definition Blu-ray devices available [3]. Since this class of semiconductors was first made, their best value was their ability to host a variety of dopant materials, most importantly rare earth (RE) elements [4].

III-Nitrides belong to the wider category of the III-V compounds in which other elements from group V such as Arsenic and phosphorus are bonded to group III elements as highlighted in figure 1. III-Nitride materials are compounds formed by the bonding of elements from group III such as Boron, Gallium, Aluminum or Indium with the group V element Nitrogen. The III-Nitrides, such as Aluminum Nitride (AlN), Indium Nitride (InN) and Gallium Nitride (GaN), are known for having a wide range

of band gaps, extending from 0.7 eV for InN , 3.4 eV for Gallium Nitride and up to 6.2 eV of Aluminum Nitride as shown in figure 2 [5] .

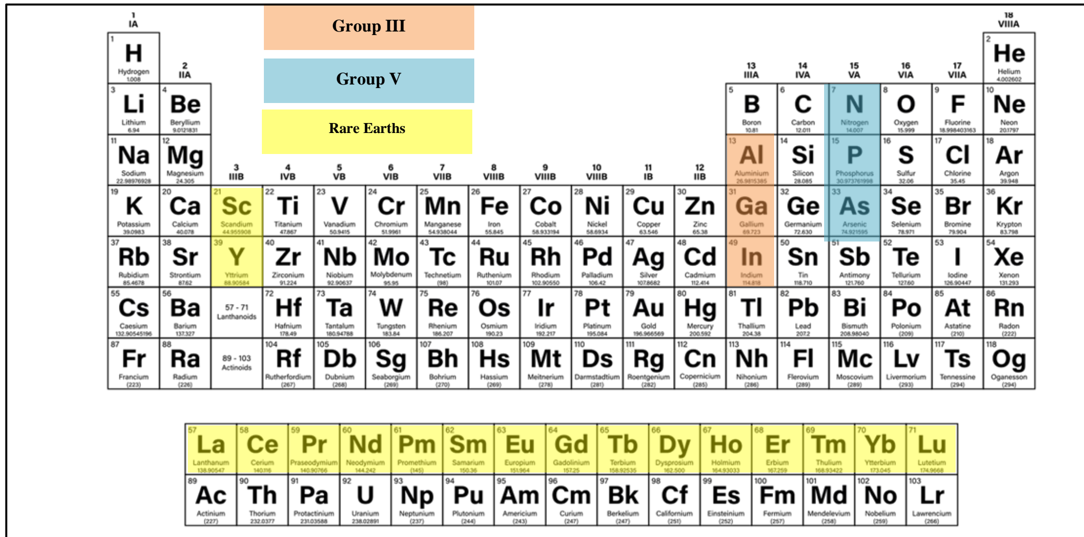

Figure 1: Periodic table of the elements with highlighted group III-V and rare earth

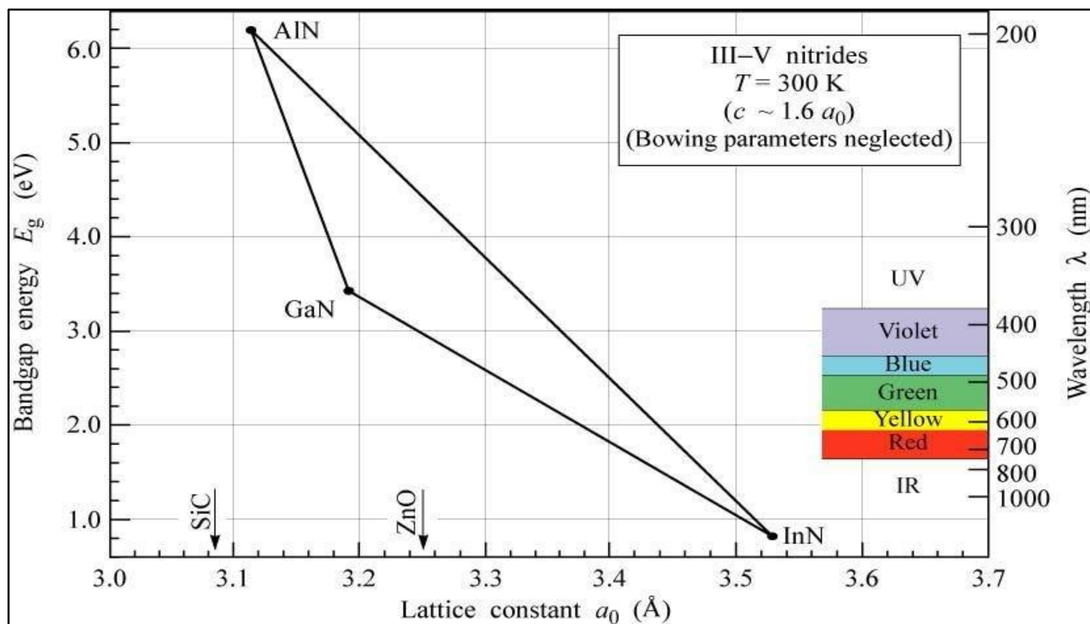

Figure 2: Band gap energies of III-Nitrides with their lattice parameters

A band gap is the amount of energy required for a charge carrier to be excited from the highest occupied energy level (valence band) to the lowest unoccupied energy level (conduction band). When charge carriers transition between these two energy levels without changing their momentum (k), the material is then said to have a direct band gap. An indirect band gap occurs when there is a change in the momentum of the charge carrier as shown in figure 3 below. This change in the momentum have to be conserved first by a release of energy as per the energy conservation principal, which significantly reduced the probability of a radiative recombination in indirect band gap semiconductors compared to direct band gap. Unlike other III-V compounds such as Silicon carbide (SiC) and Gallium phosphide (GaP), III-Nitrides have direct bandgaps which makes them a much-preferred choice for optical applications due to the fact that the entire energy absorbed for excitation of the carriers is released upon recombination without having to compensate for the momentum difference.

Ternary structures of III-Nitrides also exist such as Indium Gallium Nitride (InGaN) and Aluminium Gallium Nitride (AlGaN), these alloys provide the possibility to tune their band gaps to meet different needs in optoelectronics and photovoltaics. Alloying III-Nitrides allow for the coverage of wider regions of the electromagnetic spectrum (UV-Vis and infrared) what makes them fitting the criteria for applications in solid state optoelectronic devices such as light emitting diodes (LEDs) and Laser diodes (LDs).

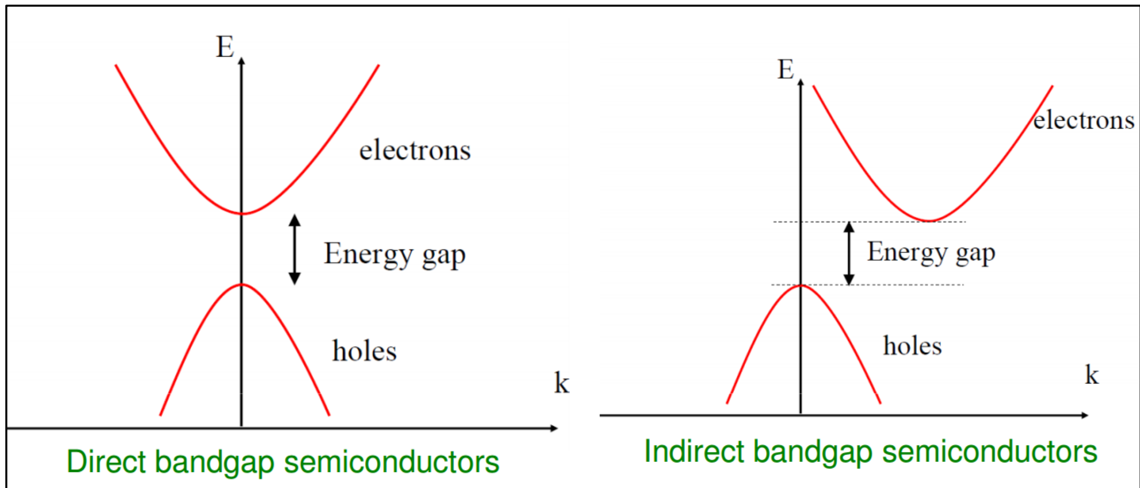

Figure 3: An illustration of the difference between direct and indirect bandgap

Exceptional developments in the III-Nitride field have been made especially in the last 30 years, their highly attractive properties made it possible to make outstanding breakthroughs in blue to UV LEDs and LDs, as well as optimized high frequency transistors. In addition, the wide range of band gap energies makes their absorption edge variable and can be optimized to be applied in solar cells.

Rare earth (RE) elements have always been naturally selected candidates to serve as active ions in many solid-state applications because of their wealth of optical properties making them applicable in almost all of the electromagnetic spectrum. RE elements are the 15 lanthanides of the periodic table in addition to Scandium and Yttrium elements. These RE elements have their *4f* energy levels occupied by electrons from 0 (La) to 14 (Lu) this occupancy of the *4f* shell is what gives them their unique optical properties. One of the most intensively studied RE elements is Erbium (Er). Er is characterized by a partially filled *4f* level. This deep laying core level has an intrinsic spectral emission that is highly shielded by the overlaying electrons of the *4p* and *5p* shells. This shielding effect protects the emission of the 4f level from being affected by the surroundings of the atom. Erbium ion (Er^{3+}) has an electronic transition from the

first excited energy state $^4I_{13/2}$ to the ground energy state $^4I_{15/2}$, this transition is of high value for optical devices operating around the 1.54μm wavelength emission. This emission is highly important for telecommunication devices, specifically in the optical fibers because it falls within the minimum loss window for this material.

III-Nitride materials have been viewed as attractive host semiconductor candidates for high efficiency optoelectronic applications. This is because of their chemical and physical properties such as direct and wide bandgap, strong chemical bonds, high melting point and high thermal conductivity. Aluminum nitride (AlN) and Gallium nitride (GaN) are two III-Nitrides with high potentials to serve as host materials for Er ions as well as other RE elements. These two compounds, AlN and GaN, have direct bandgaps of energies 6.1 eV and 3.4 eV at room temperature, respectively. Doping them with Er creates Er-Doped AlN and Er-doped GaN epilayers that showed significant reduction in thermal quenching problem which highly affects the intensity of the 1.54μm emission of Er^{3+} ions at room temperature.

It has been demonstrated that the thermal quenching for Er emission intensity at 1.54μm is substantially lower in GaN (E_g = 3.4 eV) as host material comparing to other smaller bandgap host semiconductors such as Silicon (Si) (E_g = 1.12eV) and Gallium Arsenide (GaAs) (Eg = 1.43eV) which was reported by C. Ugolini et al. [6]. Furthermore, it was reported by T. M. Altahtamouni et al. that, at room temperature, Er emission intensity using AlN (Eg = 6.1 eV) as a host material is higher than GaN [7]. However, the Er emission intensity at 1.54μm form these epilayer structures is weak and not suitable for practical applications in optoelectronic devices, in other words, the quantum efficiency (QE) of the 1.54μm emission in AlN:Er, and GaN:Er needs to be improved to enable practical applications. In order to improve the QE of the targeted

PL emission, the excitation efficiency of the Er^{3+} optical centers need to be improved. This improvement can be achieved by employing quantum well (QW) structures [8]. Quantum wells are a type of nanomaterials that provide carrier confinement in two dimensions, i.e., carriers can only propagate in two dimensions rather than three. The effect of quantum confinement is achieved when the quantum well thickness is comparable to the de Broglie wavelength of carriers (electrons and holes), which leads to having discrete energy levels [9]. Once this space confinement is realized, quantum behavior is improved, and carriers become two dimensionally confined. However, a single quantum well will not provide a strong enough signal to be used in solid state device applications, so it is necessary to use a bundle of quantum wells such structure is can multiple quantum wells (MQWs) [10].

1.2 Aluminum Nitride (AlN)

Aluminum Nitride is a pale-yellow covalent compound that was first synthesized in the 1877 by the carbothermal reduction of Aluminum oxide in the presence of Ammonia or Nitrogen gas. The physical and chemical properties of AlN are listed below in Table 1. AlN is a stable compound under inert atmosphere for a temperature reaching up to 2200°C at which it melts, while it only withstands 1800°C under vacuum before decomposing. Thin oxide layers (5 nm-10 nm) can form on the surface when heated to above 700°C in air [11]. AlN possesses many valuable mechanical and electronic properties such as its high hardness and thermal conductivity.

Table 1: Some chemical and physical properties of Aluminum Nitride (AlN).

Physical property (Unit)	Value
Molar Mass (g/mol)	40.9
Density (g/cm^3)	3.260
Melting point (°C)	>3000
Boiling point (°C)	2517
Thermal conductivity (W/cm.K)	2.0
Electron mobility (cm^2/Vs)	300
Band gap energy (eV)	6.2
Refractive index	2.2
Lattice constant (Ǎ)	^{a}3.11 – ^{c}4.97

The most stable and abundant crystal structure of AlN is the hexagonal wurtzite (WZ) structure in which each Al atom is covalently bonded to 4 nitrogen atoms in a tetrahedral geometry. Figure 4 shows the hexagonal wurtzite structure of AlN in which the lattice parameters (a) and (c) are 3.11 Å and 4.98 Å, respectively. The 4 N atoms are connected to the Al atom by two types of bonds, one bond type is 1.1917 Å long and is parallel to the c-axis and the other type is 1.885 Å and these represent to the three-tetrahedron legs. This crystal structure is the source of the thermal and chemical stability of AlN. Other possible crystal structures of AlN are the zinc blend (ZB) and rocksalt atomic structure. However, WZ is the most stable structure. in addition to the promising features of AlN, a major interest is in its ability to alloy with GaN to for the ternary compound AlGaN which is heavily employed in optical and electronic devices [11].

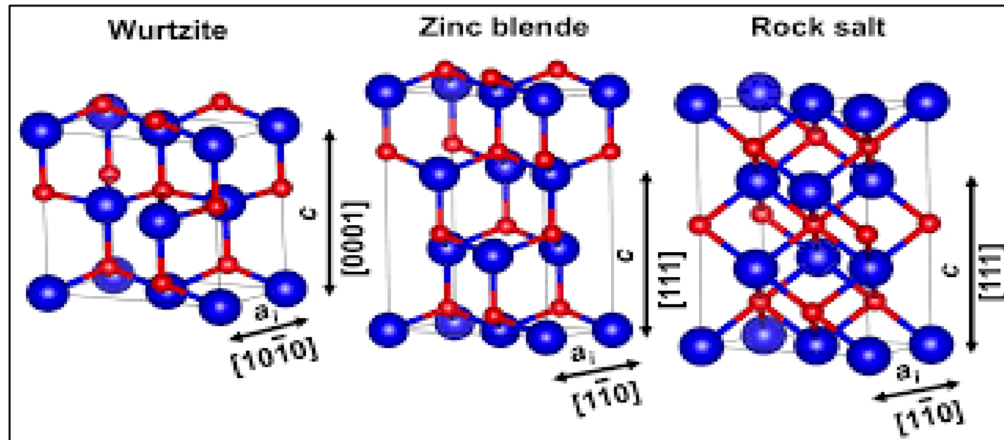

Figure 4: Possible crystal structures of AlN and GaN

1.3 Gallium Nitride (GaN)

Gallium nitride (GaN) is a pale-yellow colored wide bandgap semiconductor with a direct bandgap of 3.4 eV as shown in table 2. GaN is a completely synthetic material meaning that it cannot be found in nature [12] and was first synthesized by Maruska and Tietjen in 1969 by employing hydride vapor phase epitaxy [13]. However, it wasn't until 1991 that the real potentials of this semiconductor were unleashed with the development of metalorganic chemical vapor deposition technique [12][14]. This technique made it possible for the heteroepitaxial growth of GaN on large surface area substrates such as sapphire, ultimately enabling the determination of p-type doping mechanism for GaN. Just like AlN, GaN is tetrahedrally bonded, with bond energies of 8.9 eV/atom which is considered high in comparison with other III-V compounds. This strong bonding resulted in the relatively high melting point listed in table 2 as well as the good thermal conductivity [15]. GaN, as it is the case with the previously discussed AlN, has two possible crystallization structures, zinc blende and Wurtzite with the later structure being the more thermodynamically favored form.

Table 2: Chemical and physical properties of Gallium Nitride GaN

Physical property (Unit)	Value
Molar Mass (g/mol)	83.7
Density (g/cm^3)	6.1
Melting point (°C)	>2500
Thermal conductivity (W/cm.K)	1.3
Electron mobility (cm^2/V.s)	1500
Band gap energy (eV)	3.4
Refractive index	2.35
Lattice constant (Ǎ)	^{a}3.18 – ^{c}5.18 [10]

In this study, Er-doped AlN/GaN multiple quantum well structures (AlN/GaN:Er MQWs) are synthesized by metalorganic chemical vapor deposition. To assess the ability of this structure to enhance the QE of the 1.54μm emission of Er^{3+} ions compared to AlN:Er and GaN:Er epilayers photoluminescence spectroscopy was used. Scanning transmission electron microscopy (STEM) was used to examine the nanostructure's morphology, its interplanar spacing, diffraction patterns and also elemental analysis using the coupled electron dispersive spectrometer (EDS). Surface analysis was also done using Time-of-Flight Secondary Ion Mass spectroscopy (Tof-SIMS) which provided information about the doping material Er. The structure's crystalline quality was studied by X-ray diffraction (XRD). Finally, the optical properties were studied using Raman spectroscopy.

CHAPTER 2: LITERATURE REVIEW

2.1 Rare-earth (RE) elements and RE doped semiconductors

The term Rare-earth or **Rare-earth metals** is defined by the international union of pure and applied chemistry (IUPAC) as a group of 17 elements of the periodic table which are all sharing similar physical and chemical properties which results in them being usually found in the same deposit ores. They include the lanthanides (elements with atomic numbers (z) ranging from 57 to 71) in addition to Scandium (z=21) and Yttrium (Z=39). The nomenclature ***Rare-earth metals*** accurately describe this group as being "***rarely***" found in earth's crust in their pure metallic or minerals form and not to their relative abundance. In fact, the RE element Cerium (Ce) is more abundant than copper and some other elements are even more abundant than silver and lead.

Rare-earth (RE) doped semiconductor materials have been widely investigated and studied for the exquisite properties they provide as dopants. Doping with lanthanides and actinides, especially with elements like Erbium (Er), Europium (Eu) and Neodymium (Nd) have been a successful approach towards better performing optoelectronic devices. These devices are used to convert light to electricity or electricity to light, and machines that incorporate this concept are all called optoelectronics.

2.2 Electronic configuration of Rare-Earth metals.

Rare earths, as mentioned before, are located in the f-block area of the periodic table with the exception of Sc and Y where both belong to the *d*-block elements. The electronic configurations of Sc and Y are [Ar] $3d^1$ $4s^2$ and [Kr] $4d^1 5s^2$, respectively. Moving on to the larger group of lanthanides, these element's electronic configuration share a Xenon core with the general form of [Xe] $4f^n$ $6s^2$ with the value of n ranging from zero to fourteen. Exceptions to this pattern are found in elements: Lanthanum where the configuration is [Xe] $5d^1$ $6s^2$, Cerium with a configuration of [Xe] $4f^1$ $5d^1$

$6s^2$, Gadolinium with a configuration of [Xe] $4f^7$ $5d^1$ $6s^2$ and lastly, Lutetium with [Xe] $4f^{14}$ $5d^1$ $6s^2$ configuration.

It is known that RE elements have a *4f* wavefunction that is highly shielded and confined in space by the subsequent $5s^2$ and $5p^6$ electrons, this confinement allowed the 4f to have intra-shell transitions that give rise to unperturbed emission lines when the RE is incorporated in a host material such as a semiconductor. The occupancy of the *4f* shell is what gives lanthanides their special properties making them of great interest in various optoelectronic applications. Although, Sc, Y and La lack the partially or fully filled *4f* level, they still exhibit similar physical and chemical properties as the other 14 elements from Ce to Lu due to their analogous electronic configuration to lanthanum. Although these elements have similar electronic structures, however, the minor differences in their structures gives uniqueness to each of them, illustrated in a diversity of optical properties. To further understand the properties of lanthanides, it is important to follow their electronic configuration in their metallic and ionic forms. Table 3 below shows the electronic configuration of lanthanides along with the configuration of their most important and valuable ionic form, the trivalent cation (Ln^{3+}). While the majority of lanthanides share the Xenon core, the fully filled *6s* orbital and the partially filled *4f* orbital, four elements skip the rule by having a single electron in the *5d* orbital, namely La, Ce, Gd and Lu. The *5d* orbital tends to be filled before the *4f* in these 4 elements to achieve a much energetically stable configuration, that when ionized give rise to 4f orbitals that are empty, half-filled and fully-filled for La, Gd and Lu, respectively.

Table 3: Electronic configuration of rare earth atoms and theri trivalent cations.

Element	Electronic configuration	
	Atom	Trivalent cation (3+)
La	[Xe] $5d^1$ $6s^2$	[Xe]
Ce	[Xe] $4f^1$ $5d^1$ $6s^2$	[Xe] $4f^1$
Pr	[Xe] $4f^3$ $6s^2$	[Xe] $4f^2$
Nd	[Xe] $4f^4$ $6s^2$	[Xe] $4f^3$
Pm	[Xe] $4f^5$ $6s^2$	[Xe] $4f^4$
Sm	[Xe] $4f^6$ $6s^2$	[Xe] $4f^5$
Eu	[Xe] $4f^7$ $6s^2$	[Xe] $4f^6$
Gd	[Xe] $4f^7$ $5d^1$ $6s^2$	[Xe] $4f^7$
Tb	[Xe] $4f^9$ $6s^2$	[Xe] $4f^8$
Dy	[Xe] $4f^{10}$ $6s^2$	[Xe] $4f^9$
Ho	[Xe] $4f^{11}$ $6s^2$	[Xe] $4f^{10}$
Er	[Xe] $4f^{12}$ $6s^2$	[Xe] $4f^{11}$
Tm	[Xe] $4f^{13}$ $6s^2$	[Xe] $4f^{12}$
Yb	[Xe] $4f^{14}$ $6s^2$	[Xe] $4f^{13}$
Lu	[Xe] $4f^{14}$ $5d^1$ $6s^2$	[Xe] $4f^{14}$

Moreover, the *4f* electrons are effectively shielded from the surrounding ligands attraction by the inner $5s^2$ and $5p^6$ shells, resulting in a weak crystal field strength on the 4f electrons. This shielding prevents the *4f* electrons from participating in bond formation and only leaves it to the $6s^2$ and $5d^1$ orbitals to determine the lanthanide's valency. Because of the shielding, *4f-4f* transitions are significantly sharp in Ln^{3+} species. The transition of an electron from a low energy *f* orbital to a higher energy *f* orbital is defined as an *f-f* transition of an intra-*f* transition. For the case of lanthanides,

these transitions happen within the *4f* orbital thus called intra-*4f* transitions. The *4f* energy levels of lanthanides are characteristic of each ion and are effectively isolated from the environment of the ion, and the properties of these transitions are affected by the nature of their host [16]. Since the realization of the abilities of lanthanides, continuous efforts are done to utilize them in the optoelectronics field.

2.3 Excitation mechanisms of rare-earth doped III-Nitrides.

Excitation mechanisms of rare earth dopants in III-Nitrides is a very important topic to be understood in order to have a strong understanding of the luminescence properties of this class of materials. Even though the excitation mechanisms of RE ions have been granted a large share of studies throughout the years to try and conclude a general excitation mechanism for all of the optically active RE ions, it is still a difficult task to assign one general mechanism to apply for all REs. However, it is believed that the excitation mechanism of each RE ion is different from the others and should be studied case by case because of the multiple routs excitation energy can be delivered to RE ions. The fact that the *4f* shell of all of the RE^{3+} ions is highly shielded by the overlaying *5s* and *5p* orbital and it being deeply "Hidden" is the biggest obstacle on the way of understanding the excitation mechanism.

Many attempts have been done to try and reveal the mechanism of transferring kinetic energy from the host material to the RE ion's *4f* core, and it has been well established that the RE ion in the III-V compound replaces the III ion side and play the role of an isoelectronic structured trap [17]. An isoelectronic trap is an impurity that contains the same number of valence electronic structure as the replaced species. So, because all of the RE^{3+} have the outer electronic configuration of $5s^2$,$5p^6$ which is the same as the III-column ions outer configuration, RE^{3+} is called an isoelectronic impurity when it exchanges the III ions in their compounds.

In general, the excitation mechanisms can be divided into two main categories: Direct excitation mechanisms and indirect excitation mechanisms. Firstly, the direct excitation mechanisms are those based on pumping excitation energy that resonates with the energy difference between the ground state of the *4f* shell of a RE ion and its excited state. In rare cases that this mechanism is successful due to the shielding of the 4f level that results in very weak absorption cross section, but advances in diode laser technology and the simplicity of this method can produce some successful attempts [18][19]. On the other hand, indirect excitation mechanism uses an intermediate called the sensitizer to deliver the excitation energy to the RE ion. This sensitizer has a high absorption cross section within a certain spectral range and can be used to deliver the excitation energy to the RE ion efficiently. Usually, the hosting material (its lattice) is used to play the role of a sensitizer instead of incorporating other ions to the structure and causing more complicated outcomes to be studied. Our focus will be mainly on the indirect excitation mechanism by energy transfer from the surrounding lattice to the RE ions in III-nitrides.

Some of the suggested excitation mechanisms are:

i. *Band-to-band excitation rout:*

in this mechanism, electron-hole pairs are generated from the excitation of electrons from the valence band (VB) to the conduction band (CB) of the host material by either the resonant pumping of photons with energies equal to or larger than the bandgap energy of the host, or by applying hot electrons in methods like cathodoluminescence, and electroluminescence. Therefore, free excitons are created and can interact with and transfer their energy to the RE (for example Er^{3+}).

ii. *Below-bandgap excitation:*

This mechanism goes by using excitation photons with lower energy than the bandgap energy of the host material, which will result in exciting the localized or extended defects within the structure. Thus, the excited carriers can be trapped by the impurities (REs or defects) and form bound excitons (BEs) or bound carriers coupled with free carriers (B-F). RE ions can be excited if the recombination of these BEs or (B-F) resulted in the release of an amount of energy that is at least equal to the energy difference of the core levels of the RE ion, and if the recombined defects are close enough to the RE [20]. This excitation mechanism is considered to be the most prominent and most expected pathway of Er^{3+} (and other REs) excitation [17].

2.4 Erbium doped Semiconductors

In the early stages of developing light emitting devices, scientists focused their efforts in developing infra-red light emitting diodes due to the limitations in host materials. Only semiconductors with narrow optical bandgaps were sufficiently available with considerable purities. Most of these devices were based on the intra-*4f* transition from the ground state to the first excited state. Dieke and his colleagues precisely determined the energy levels of the *4f* electrons of lanthanides in 1968 by experimentally investigating the optical spectra of RE ions individually doped into $LaCl_3$ crystals (host) [21]. This approach is applicable to other hosts as well due to the earlier discussed shielding effect on the *4f* levels, which renders them entirely unaffected by the nature of their surroundings. This study by Dieke was further extended to higher energy levels by Ogasawara in 2004 [22] resulting in the Dieke diagram shown in figure 5 . The element Erbium (Er) has gained the interest of researchers in optical communication field due to its properties. According to [23], the trivalent (Er^{3+}) ion produces an emission from the $^4I_{13/2} \rightarrow {}^4I_{15/2}$ transition and this

emission is at the wavelength 1.54 μm. When doped in a semiconductor host, this produced wavelength is of great importance in silica based optical fibers as it lies within the minimum loss window for the optical fibers and is several times more eye-safer than that of Neodymium based emissions [24]. Moreover, this energy transition of Er^{3+} matched the absorption minimum of silicon dioxide (SiO_2) which is the main constituent for optical fibers. Thus, it was very clear towards which direction efforts must be shifted, especially that the commercial aspect appeared to be very attractive and promising. Semiconductors doped with Er^{3+} took the lion's share of scientific publications related to optoelectronics[25] [26][27] [28].

Although the wavelength of the intra-*4f* shell transition emission is not affected by the semiconductor host, its intensity is greatly affected by the nature and composition of its surrounding. When doped in semiconductors having low band gaps, the intensity of Er^{3+} emission decreases as the temperature increases, this thermal quenching limits the quantum efficiency of this highly important emission. This thermal quenching effect can be limited if the Er is in a host material that has a larger energy gap and an ionic nature ,as it was proved by [29]. This suggested that III-Nitride materials would create an excellent environment for an enhanced 1.54 μm emission. The findings of [29] are shown in figure 6, where the effect of temperature increase on the photoluminescence intensity of Er doped semiconductors is clear. Gallium nitride with its 3.4 eV direct bandgap have a stable PL intensity throughout the testing temperatures varying from 2K to 600 K while all other semiconductors decayed after exceeding 100K. This resulted in making GaN an interesting candidate to host Er and other RE elements such as Eu.

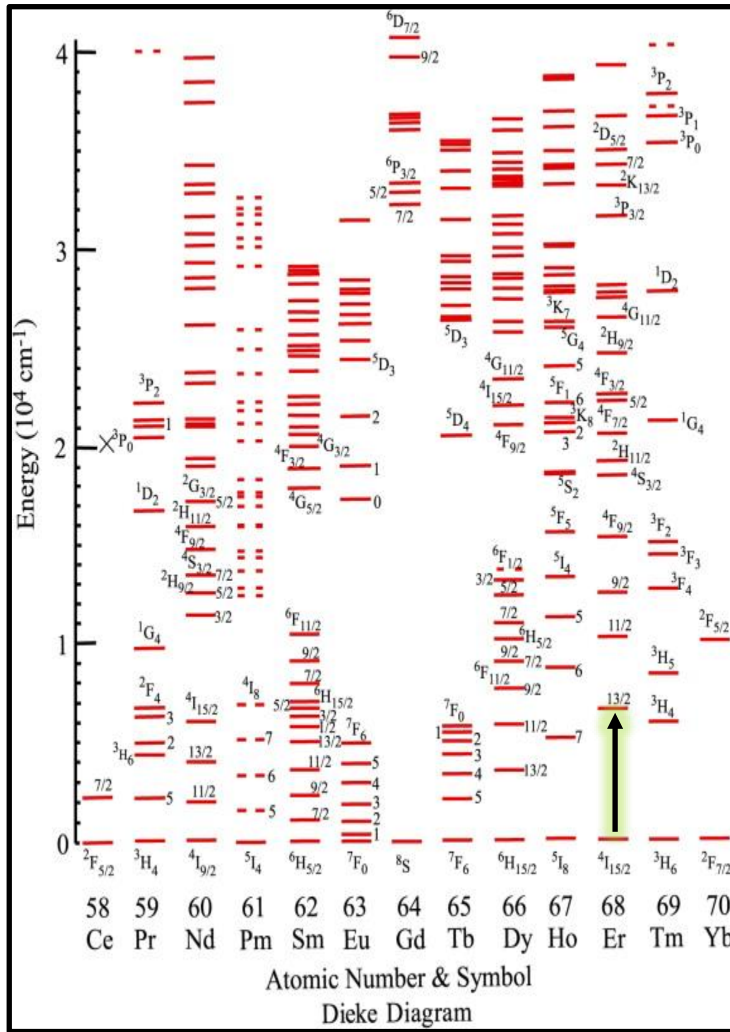

Figure 5: Dieke Diagram.

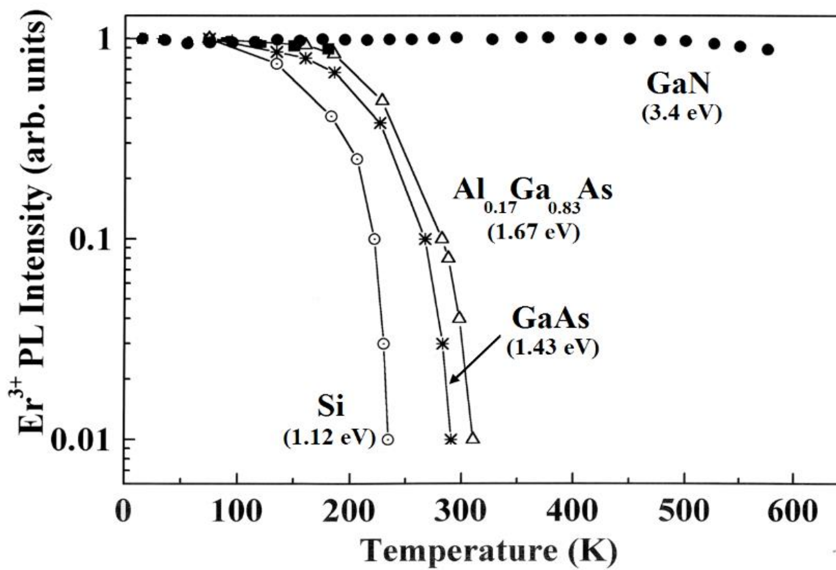

Figure 6: Effect of Temperature on the PL intensities of some Er doped semiconductors.

2.5 Er-Doped AlN and GaN

AlN and GaN have been intensively studied in the past and recent years. Thin films of RE doped and undoped AlN and GaN were synthesized and grown using cutting-edge growth techniques such as molecular beam epitaxy (MBE), plasma enhanced or thermal atomic layer deposition (ALD), magnetron sputtering, and metalorganic chemical vapor deposition (MOCVD). Various studies reported the growth of AlN and GaN on different types of substrates such as sapphire (Al_2O_3), silicon, hexagonal 6H-silicon carbide, and GaN [30][31][32]. Although homo-epitaxial growth (using substrate of the same grown material) of semiconductors leads to producing high quality thin films, it's not always the most efficient way. While bulk GaN and AlN may seem like the best choice for growing these two materials, their small size and expensiveness prevents their large-scale application, hence, other types of substrates were used. The choice of substrate is made mainly so that the lattice mismatch between the grown film and the substrate is as low as possible, to prevent formation of dislocations and other crystal defects that can greatly affect the quality of the film. SiC has a lattice mismatch with GaN of only ~3.5%, while sapphire has a 16% mismatch with GaN, this suggest that SiC is best choice for such process, however, because the prices of commercially available SiC substrates are much higher than that of sapphire, this makes the choice of sapphire as a substrate more commercially favorable [33]. Supported also by the fact that the performance of III-N based devices was found uninfluenced by the resulting dislocations as much as other III-V SC such as GaAs and InP [34], we use a c-plane sapphire substrate for this study.

Various studies have been done on Er doped AlN and GaN epilayers investigating their various properties such as structural and optical properties including photoluminescence properties. The first study to investigate the PL emission of Er^{3+}

ions at 1.54 μm in MBE grown AlN and GaN thin film hosts was done by [26] in 1994, the study observed the PL emission at various temperatures and found that the emission intensity of Er doped GaN on sapphire substrate is as strong at 300K as it is at 6 K and 77 K with a negligible loss in the PL intensity due to temperature effect. Another study by (Rinnert, et. al) reported the growth of Er-doped AlN thin film on Si substrate by RF magnetron sputtering and the effect of Er% on the PL intensity of Er emissions in the visible and IR range of the spectrum, the report showed that the Er% was optimized for PL emission at 1at% [35] . This shows that increasing Er% results in a concentration-driven quenching of PL intensity. However, it was only in 2007 that the synthesis of Er doped GaN epilayer by metalorganic chemical vapor deposition was realized as a result of the advancement of MOCVD technology which allowed the utilization of the metal organic Er precursors which are characterized by their low vapor pressure at room temperature. This accomplishment was achieved by H. Jiang, J. Lin, C. Ugolini and J. Zavada, where their produced epilayers of GaN:Er showed sharp PL emission peaks at 1.54 μm with very minimal thermal quenching effect showing only 20% decrease between 10K and 300K [36].

A more recent study was done on MOCVD grown AlN:Er, the study first investigated the effect of different growth temperatures of AlN:Er layer on the PL intensity and it was found that the optimal PL emission was obtained at 1050 °C. Following that the performance of this AlN:Er was compared to a GaN:Er epilayer in terms of enhancing the 1.54 μm emission . Similarly structured epilayers of AlN:Er and GaN:Er with Er doped layer of 500 nm were grown on sapphire substrates. Its results showed that AlN:Er epilayers had higher PL intensities at the 1.54 um wavelength than GaN:Er. This was explained by the fact that AlN has a higher resistance to thermal quenching than GaN owing this to its larger optical band gap [7].

2.6 Quantum Well structures

III-Nitrides such as GaN and AlN have energy gaps of 3.4 eV and 6.2 eV, respectively [5], and doping them with Er to create Er-doped GaN (GaN:Er) and Er-doped AlN (AlN:Er) epilayers showed a significant reduction in the thermal quenching. However, there was still the problem that the quantum efficiency (i.e the intensity of emission governed by the ratio of emitted photons to absorbed photons.) of these structures is lower than it is needed for practical applications , and solutions to increase the QE of the Er-doped III-Nitrides are sought [25]. Improving the QE of the Er ions' emission means that it is required that the frequency of the *4f* excitation to be increased, this can be achieved by enhancing the confinement and the density of state of the carrier species, which can be done by employing a quantum well (QW) structure.

A quantum well structure, as illustrated in figure 7, is a nano-sized potential well in which charge carriers (i.e., electrons and holes) are confined in a two-dimensional region of space. This space confinement is achieved when the thickness of the well is lowered down to approach the *de Broglie* wavelength of the electrons and holes [9], once the spatial confinement is achieved, quantum behavior is improved and the electron-hole pairs become 2D confined carriers.

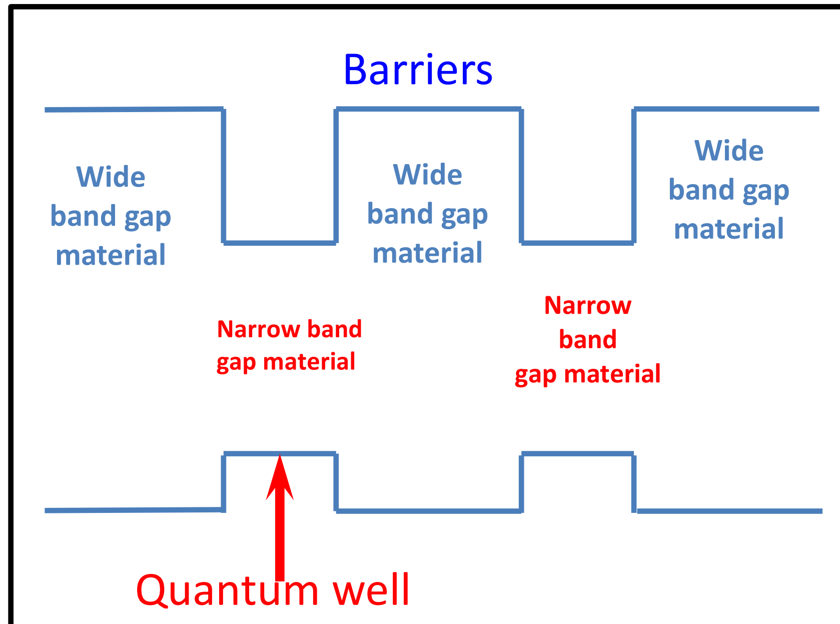

Figure 7: Visual representation of the structure of quantum wells.

Quantum wells are heterostructures, meaning that they are made by the joining two different semiconductors for example, AlN and GaN. An important requirement is that the two materials have different energy gaps, one material having a low bandgap energy (well) is sandwiched between two layers of another material with a larger optical bandgap. The material with a larger bandgap acting as the edges of the potential well inside which charge carriers are trapped, is referred to as the barrier. Widely studied semiconductors for heterostructures such as quantum wells include III-V compounds such as GaAs, InGaAs and also GaN, AlN, and AlGaN [37]. However, a single quantum well generally produces a signal that is far too weak to be used in a solid-state device applications, for that matter, it is necessary to use a collection of quantum wells, and such structure is called multiple quantum well (MQW) [10].

Multiple quantum well structures of AlN/GaN:Er have been studied previously with a clear concentration on enhancing the 1.54 µm emission of Er^{3+}. V. X. Ho and his colleagues synthesized an Er doped GaN/AlN quantum well structure composed of

200 periods of 2 nm thick GaN:Er grown by MOCVD. By employing a technique called variable strip they were able to achieve an optical gain up to 170 cm^{-1}, the structure proved to increase the intensity of the 1.54 µm by an order of magnitude compared to Er doped GaN [24]. Another publication by T. M. Altahtamouni and others, reported the enhancement of the 1.54 µm emission of Er ions in AlN/GaN MQWs prepared by MOCVD as well. The study compared different thicknesses of wells and barriers and their PL intensities revealed that the optimum well width lies between 1 nm and 1.5 nm [8].

Although these studies, among others, have achieved enhancements in the PL emissions of Er ions, but the number of reports on Er doped MQW structures is still considered very few. In addition to that, the characterization of the synthesized MQWs needs more attention. It is crucially important to study the nano-structural properties, and optical behavior of these MQWs. In this context, the capability of MOCVD grown AlN/GaN:Er MQW structures for improvement of the IR emission of Er^{3+} at 1.54 µm will be evaluated in comparison to GaN:Er and AlN:Er epilayers. Furthermore, in addition to XRD scans and PL, the Er doped MQWs will be further studied and characterized using techniques that are not yet reported in literature such as scanning transmission electron microscopy (STEM) where their nanostructure and diffraction patterns are uncovered. Also, Raman spectroscopy and time-of-flight secondary ion mass spectroscopy (ToF-SIMS) are employed to study the phonon modes associated with the formation of multiple quantum wells and to study the elemental composition of the structure mainly detecting the dopant Er. These characterization methods will provide important insights about the quality of the adopted growth method.

CHAPTER 3: EXPERIMENTAL METHODOLOGY

In this context, Er-doped AlN, Er-doped GaN, and Er-doped AlN/GaN multiple quantum well structures were synthesized by means of metalorganic chemical vapor deposition (MOCVD). The structural, compositional and optical properties of the MQW were studied using Scanning transmission electron microscopy (STEM) coupled by an energy dispersive spectroscopy device, X-ray diffraction (XRD), Raman spectroscopy, and time-of-flight secondary ion mass spectroscopy (ToF-SIMS). The light interaction properties were studied by photoluminescence spectroscopy (PL).

3.1 Synthesis technique: Metalorganic Chemical Vapor Deposition

Chemical vapor deposition is a technology used to synthesize materials in the nanometric size in the form of powders or films from gaseous precursors [38]. It is considered one of the most advanced and state of the art techniques for nanosized film growth. It provides the ability to control growth parameters to extreme details with very high quality of product and deposition rates. There are several variations to CVD systems depending on the deposition requirements; however, the main components are all the same. Figure 8 below shows a simplified diagram of the setting of a typical CVD system. A CVD machine consists of four main parts, these are: the gas supply system and the metal/material source, the second component is the reactor chamber where the deposition takes place, the third part is the temperature control system where the temperature of the substrate is controlled, the fourth main part is the pressure control and exhaust system which maintains the low pressure inside the reactor chamber and properly disposed the exhaust gases.

Metalorganic chemical vapor deposition (MOCVD) is a very advanced technique

by which highly pure and crystalline films can be achieved. Various III-Nitrides are synthesized from organometallic compounds bearing the targeted elements such as Al, Ga or In. For example, gallium and aluminum are deposited from trimethylegallium dimers $Ga_2(CH_3)_6$ and trimethylalluminum dimers $Al_2(CH_3)_6$, respectively.

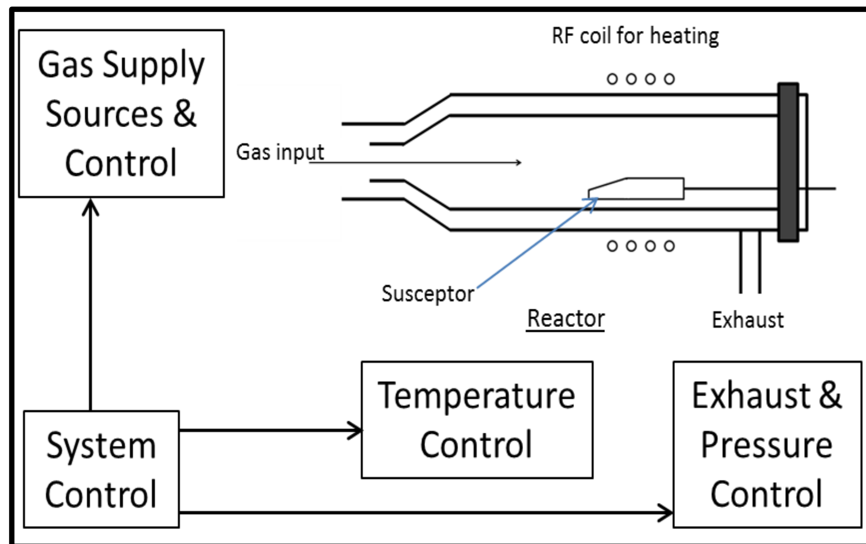

Figure 8: Diagram of a CVD system

CHARACTERIZATION TECHNIQUES

The following techniques were used to characterize the grown Er doped QWs, GaN and AlN epilayer structures

3.2 X-Ray Diffraction (XRD)

X-Ray diffraction is a very reliable analytical technique used for phase identification for crystalline materials and also for the determination of unit cell properties such as unit cell dimensions (lattice constants), and defects within the crystal structure. As shown in figure 9, an XRD machine consists mainly of an X-ray source (tube) where characteristic X-rays are produced from anodes of materials such as Cu, a sample holder and a detector. Some machines have rotating source and detector with a stable sample holder and others have only rotating sample holders.

The working principle of XRD revolves around Bragg's law shown in equation (3-1) below and visually demonstrated in figure 10. Bragg's law was developed by Sir W.H.Bragg and his son in 1913 explaining the reason behind the reflection of X-rays from crystals at specific angles of incidence.

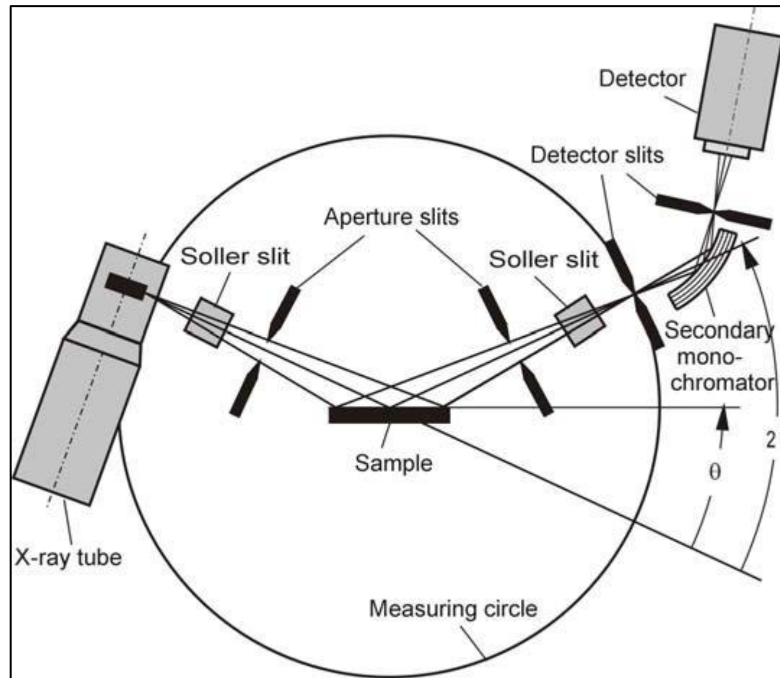

Figure 9: A schematic diagram of an XRD machine

$$n\lambda = 2d_{hkl}sin\theta$$ Equation (3- 1)

Where,

n (an integer) is the order of reflection.

λ is the wavelength of the incident X-ray.

d_{hkl} is the interplanar spacing of the crystal and (hkl) are miller indices.

θ is the angle of incidence.

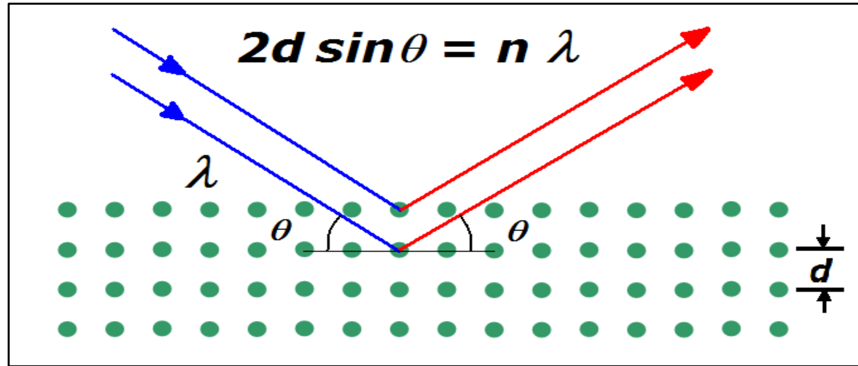

Figure 10: visual representation of components of Bragg's law.

For materials such as AlN and GaN which are exhibiting hexagonal crystal structures with lattice constants a, and c. the interplanar spacing d_{hkl} is expressed with equation (3-2) below.

$$d_{hkl} = \frac{1}{\sqrt{\frac{4}{3}\left(\frac{h^2+hk+k^2}{a^2}\right)+\frac{l^2}{c^2}}} \qquad \text{Equation (3- 2)}$$

Different varieties of XRD techniques can be found tailored for specific uses. For example, bulk materials and powder samples have their own mechanical set-ups, whereas single crystalline materials and thin films have different approaches. For thin films, grazing incidence XRD (GI-XRD), also called glancing angle XRD (GA-XRD), are used.

3.3 Raman spectroscopy

Raman is a non-destructive spectroscopy technique that provides detailed information about molecules such as the chemical structure, crystallinity and phase of molecules. It makes use of the light scattering properties of materials, where molecules scatter light coming from a highly intense laser source. In solids, the Raman effect is due to the inelastic scattering of light by the crystal vibrations which are also known as optical modes. The incoming light exchanges an amount of energy with the crystal via the creation or eradication of phonons, depending on the creation or eradication of a phonon the scattered light gains or loses a quantum of energy. The vast majority of the

scattered light is related to the wavelength of the used laser and it does not provide any useful information for the analyzer, this scattering is called Rayleigh scattering. Only a very small part of the incident light is scattered in different wavelengths and is dependent upon the molecule under study, this scattering is the Raman scattering. In Raman analysis, the shift in the energy of the scattered light is measured, thus, the characteristic value of a vibrational mode of a given material is acquired [39]. In a Raman spectrum, different peaks are seen at distinguished wavelengths with variable intensities, each peak corresponds to a particular molecular vibrational mode. These vibrational modes are characteristic which makes Raman testing useful in qualitative analysis of materials. However, these phonon modes can be shifted to lower or higher wavenumbers depending on the environment surrounding the molecule such as experiencing heat or expansion. Also lattice strains have a great role in changing the frequency of phonons, for example, a molecule experiencing compressive stress will show an increased Raman frequency in a case called blue shift where the phonon frequency shifts to higher wavenumber corresponding to a lower wavelength. In the contrary, tensile stress results in decreasing the phonon frequency towards lower frequencies which corresponds to higher wavelengths.

A Raman spectrophotometer, shown in figure 11 is typically made of an excitation source which is usually a laser, a sample illuminator and light collecting optics, a sample holder, a monochromator which is a wavelength selector tool and finally a detector (Spectrometer). The instrument used is Thermo fisher scientific DXR Raman Microscope, shown below in figure 12 with a wavelength of 532nm, 40 times scan, and the laser power is 10 using 50X microscope objectives.

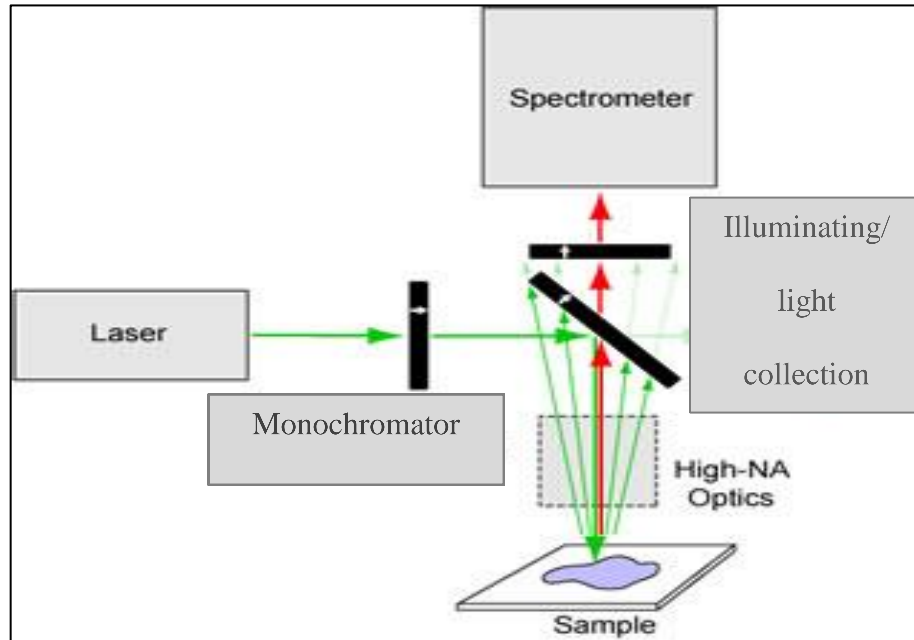

Figure 11: schematic diagram of a Raman spectrometer.

Figure 12: Thermo fisher scientific DXR Raman Microscope

3.4 Time-of-Flight Secondary Ion Mass Spectroscopy (TOF-SIMS)

ToF-SIMS is a surface sensitive analytical technique that employs a primary ion beam to investigate the surface of a solid sample. It can provide extremely reliable qualitative results about the composition of the first few nanometers of the sample's

surface [40]. A pulsed Cs or Ga ion beam bombards the surface of the material knocking out ions from the outmost top layer of the sample, these knocked out ions are referred to as (Secondary ions) as it is demonstrated in figure 13. These ions are then accelerated into a flight tube where their mass is determined by measuring the precise time by which they reach a detector (Time-of-Flight).

The sensitivity of ToF-SIMS can reach to the range of parts per billion (ppb) with a very high mass resolution, meaning that it can differentiate species with minor differences in atomic mass; this is very useful in the cases of isotopes. For this study, ToF-SIMS was mainly used to detect the presence of Er within the GaN layers of the MQWs.

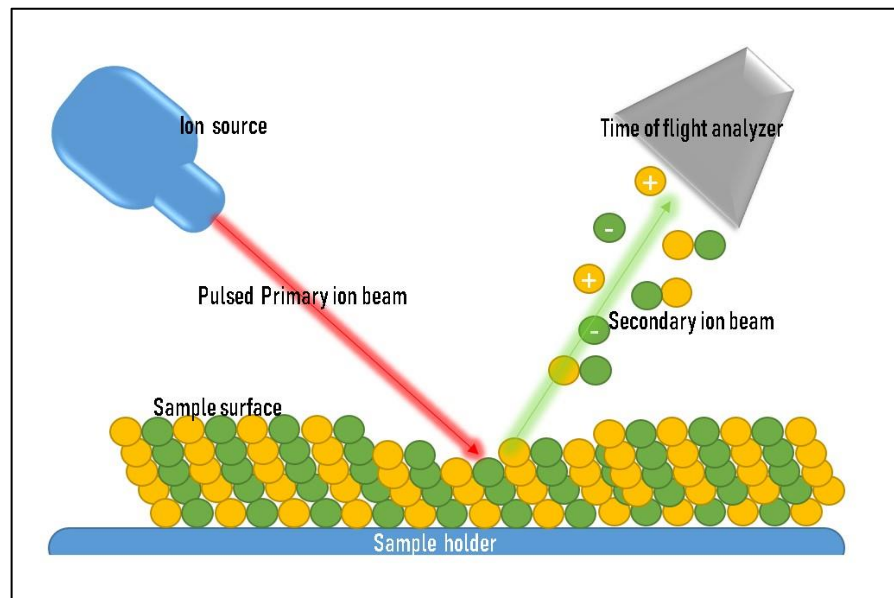

Figure 13: Illustration of the surface analysis of ToF-SIMS

3.5 Scanning Transmission Electron Microscopy (STEM)

STEM is an advanced microscopy technique developed in 1931 by Max Knoll and Ernst Ruska [41]. STEM as the name implies, uses electrons instead of electromagnetic radiation, which allows the formation of images in the nanometer scale at a significantly higher resolution than light microscopes because the de Broglie wavelength of an electron is much shorter than that of visible light. The structure of a modern STEM is demonstrated in figure 14 below. A typical STEM consists of: a vacuum system, an electron-emitting source (electron gun) with an electron accelerator, a two or three stage condensing system to focus on and illuminate a specific part of the sample, a sample holder, an objective lens which form the magnified image and an objective aperture to manipulate electrons towards the required angles, projector lenses to allow the operator to enhance the magnification as desired and finally an electron detector [42]. As shown in figure 15 in STEM, the incident beam of electrons is transmitted through the cross section of the ultrathin specimen and is then focused into a parallel detector to form the image [43]. The thickness of the STEM sample should be not more than 100 nm to allow the beam of electrons to be passed through it. These transmitted electrons are then focused and magnified by two electromagnetic lenses to be projected on a phosphor screen, which converts the information from electron into a visible form. Owing to the high resolution of STEM, even the fine crystal structure can be determined because of using the short wavelength of electron. In this study, dark field and bright field STEM was used to image the structure of the MQWs:Er, to assess visually the quality and thickness of wells and barriers, to confirm the presence of elements within their expected spaced using a coupled EDS detector, and to measure

the interplanar spaces and study the diffraction patterns of the quantum well structure.

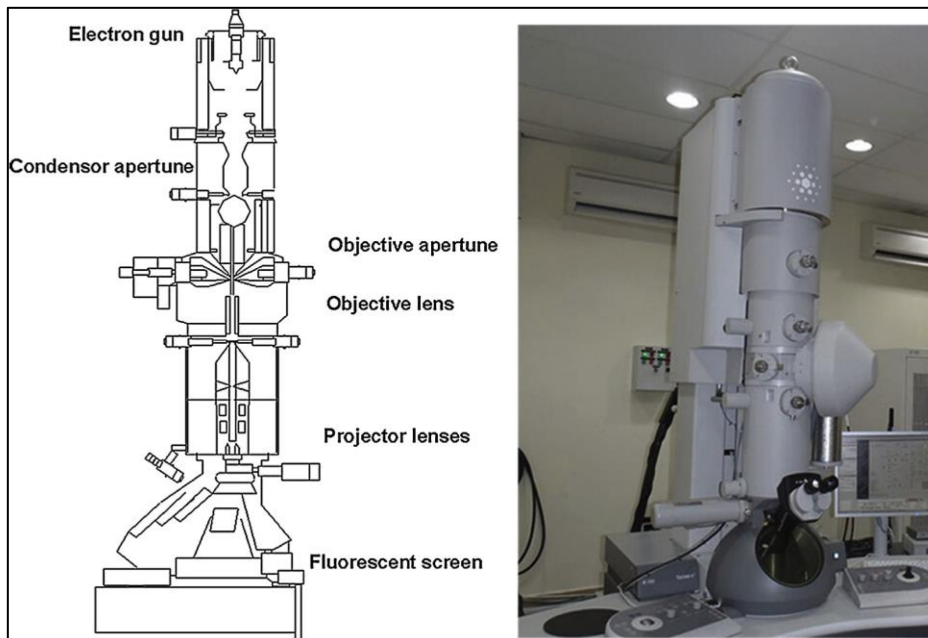

Figure 14: An illustration of a TEM (Left) and an example of a modern TEM instrument (right) [42].

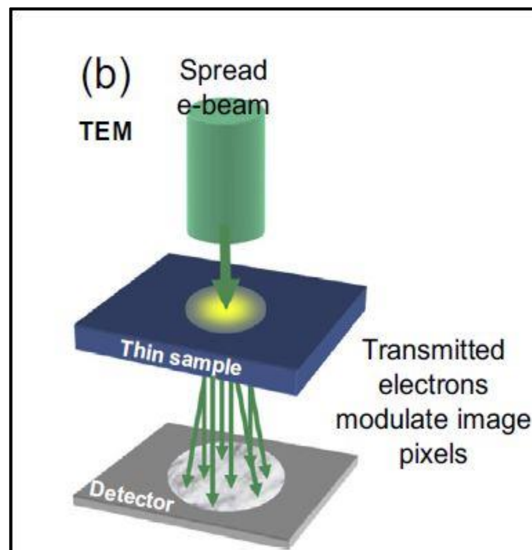

Figure 15: Image acquisition technique in TEM, Adapted from [43]

3.6 Photoluminescence Spectroscopy (PL)

Photoluminescence is a diverse and powerful nondestructive optical method used to study the electronic structure of a material. When light is directed onto a material, the energy associated with this particular wavelength is absorbed by the charge carriers (electrons). Depending on the amount of energy, these electrons can be excited to higher energy levels leaving holes behind, this excitation is called photoexcitation [44]. The excess amount of energy absorbed by the electron is then dissipated in many forms, following either non-radiative or radiative dissipation, the later one results in the production of light hence the phenomenon is called photoluminescence. Therefore, photoluminescence can be defined as the spontaneous emission of light from a material upon being optically excited. The properties of this emission, its intensity and spectral content, have direct relation to various properties of the material. When a material is photo-excited, electrons gain enough energy to move into permissible states, for semiconductors, this transition is majorly from the valence to the conduction band as shown in figure 16.

The energy of the emitted light is directly related to the difference between the two electron states, in semiconductors this is the same as the band gap energy. The quantity or intensity of the emitted light is an indication of the relative contribution of radiative routes in the total process [45].

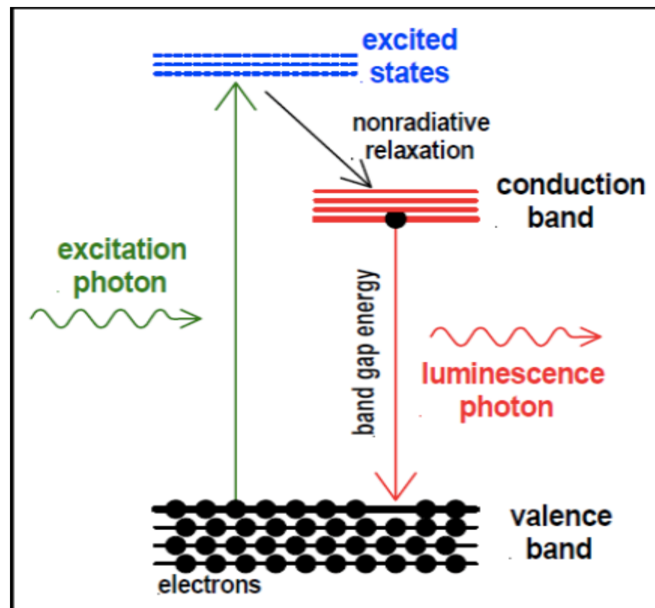

Figure 16: Principle of photoluminecence

PL spectroscopy uses a laser light for the excitation of charge carriers, this laser has to have an energy significantly larger than the optical band gap of the material. In addition to the laser light source, a PL device, which is illustrated in figure 17 generally and mainly consists of a sample stage, a monochromator which is used to filter out unwanted wavelengths allowing only the desired wavelength to pass through, and finally a detector that measures the intensity of PL emission as a function of the wavelength. A DongWoo's Maple II basic PL spectrophotometer shown in figure 18 was used for PL measurements in this work. This system had a spectral range on 539nm to 900 nm with a detector and laser source wavelength of 532 nm. Because this study needs to be done at the infrared region, the spectral range was modified to 1000nm-1700nm by upgrading some hardware parts and the software of the system.

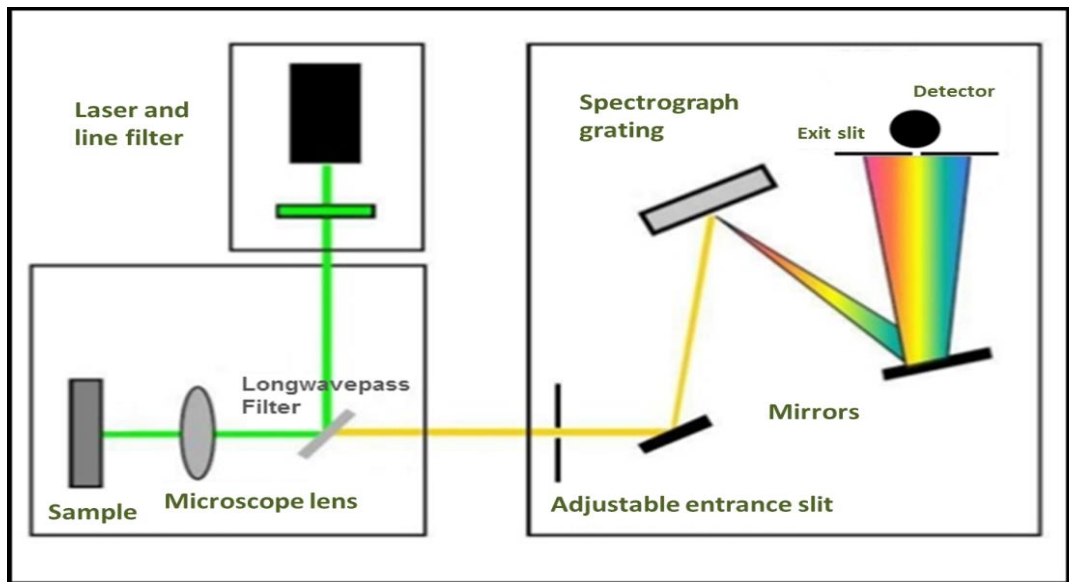

Figure 17: A schematic diagram of a PL spectrophotometer

Figure 18: Maple II PL system.

CHAPTER 4: RESULTS AND DISCUSSION

4.1 MOCVD growth of AlN:Er , GaN:Er and AlN/GaN:Er MQW structure

The structures of grown Er doped AlN and Er doped GaN grown on c-plane sapphire substrates are shown in figure 19. The growth process of Er-Doped aluminum nitride (AlN:Er) is shown in figure 20 presented as the growth temperature Vs growth time for the deposition steps. The growth process required the following materials: an aluminum source which is Trimethylaluminum (TMA), a nitrogen source that is ammonia (NH_3), an erbium source which is the organometallic compound trisisopropylcyclopentadienylerbium (TRIPEr) which was *in situ* introduced for Er doping. The carrier gas was hydrogen, and its flow rate was kept at 2 standard liters per minutes (SLM). The growth started with the deposition of two thin AlN buffer layers the first buffer layer is 30 nm thick was grown at 950°C and 30 mbar. The second buffer layer (100 nm thick) was grown at 1100°C and 30 mbar. Following theese buffer layers, a 0.5 µm AlN template was deposited at 1300°C and 30 mbar, following this template layer was the growth of the Er doped AlN layer at 1050°C with a 250 nm thickness.

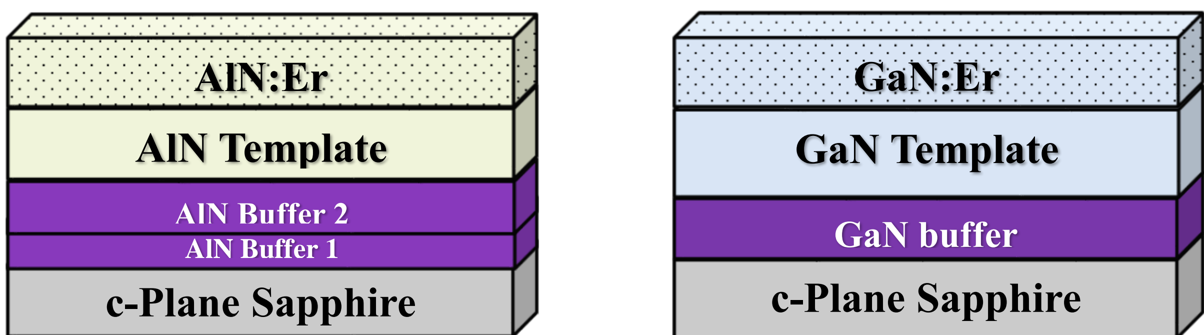

Figure 19: Structure of AlN:Er (left) and GaN:Er (right) Epilayers

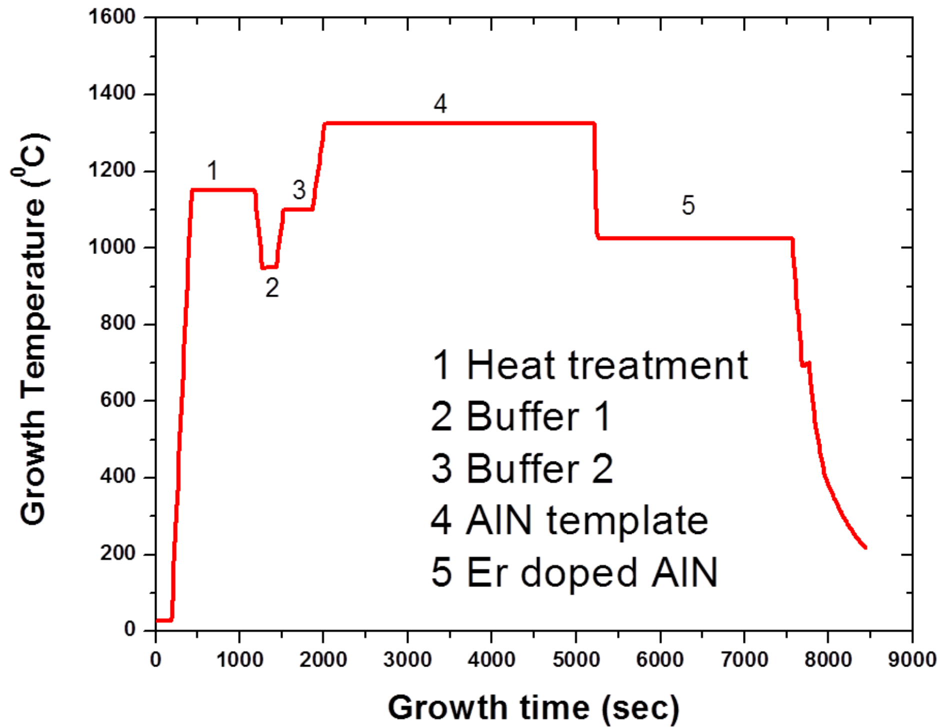

Figure 20: Growth temperature Vs growth time for the deposition of AlN:Er.

Next, the growth of GaN:Er epilayer required the following materials: for gallium source, trimethylgallium was used, and for Nitrogen introduction ammonia gas was pumped. Similarly to AlN:Er TRIPEr was used for *in site* Er doping, and hydrogen gas was used as the carrier gas and was kept at 2 SLM. The growth process started by depositing a 50 nm GaN buffer layer at a temperature of 550°C at 400 mbar. Following that, a GaN template of 1.4 µm was grown at 1060°C and 400 mbar. Finally, the Er doped GaN epilayer of thickness 250 nm was grown at 1040°C and 40 mbar.

The Er doped multiple quantum well structure (AlN/GaN:Er) was synthesized using metalorganic chemical vapor deposition method and grown on sapphire substrates. Sources of Aluminum and Gallium metals were Trimethylaluminum (TMA) and Trimethylgallium (TMGa), respectively. The dopant Erbium was obtained from the precursor Tris(isopropylcyclopentadienyl)Erbium, which was maintained inside a stainless-steel bubbler at 60°C. while Ga Precursor was stored inside the same kind of

bubbler at 3°C. Hydrogen gas (H_2) was the carrier gas used to introduce Ga and Er into the reaction chamber. Nitrogen was incorporated into the structure by pumping Ammonia (NH_3) inside the chamber.

The growth process is described in figure 21 it starts by annealing the c-plane single crystal sapphire substrate at 1150°C, then a 30 nm AlN buffer layer (buffer 1) was grown at 950°C, followed by another AlN buffer layer (buffer 2) of thickness 100 nm at 1100°C and an AlN template layer measuring 0.5 µm in thickness at 1300°C, all of these three layers were grown at 30 mbar of pressure. Then follows the growth of the 50 periods of Er doped MQWs composed of undoped AlN barriers and Er doped GaN quantum wells grown at 1000°C and 30 mbar pressure. Figure 22 below shows the structure of the MOCVD grown AlN/GaN:Er MQW structures of 50 repeating periods, where each period is an AlN barrier wall and a GaN:Er quantum well. The different properties of the MQW structure are discussed in the coming sections of this chapter.

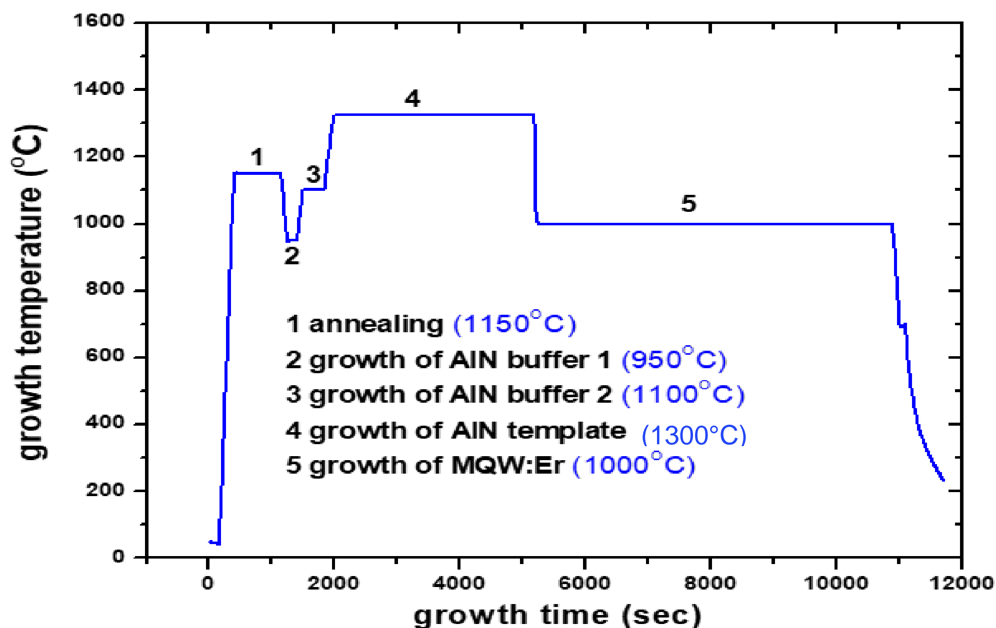

Figure 21: Growth temperature sequence of the Er doped AlN/GaN MQWs

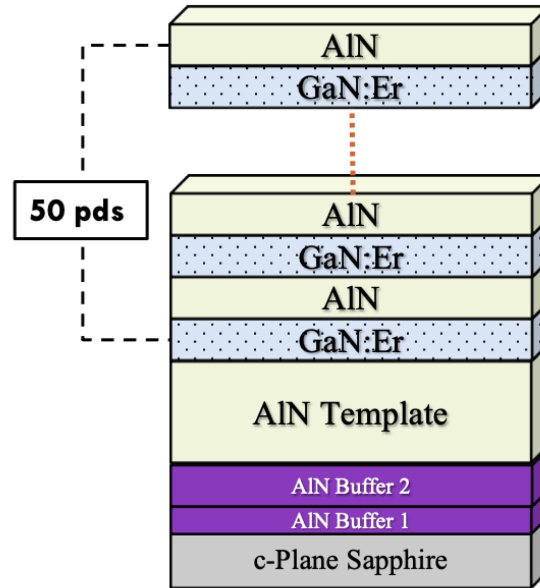

Figure 22: layer structures of the Er Doped AlN/GaN MQWs

4.2 Structural Properties

The structural properties of the grown GaN:Er, AlN:Er epilayers and the MQWs:Er were investigated by means of X-ray diffraction and Transmission electron microscopy. The earlier method provides an insight about the crystallinity and purity of the samples while the later method shows the quality of the grown MQWs in the nanoscale, their elemental composition and crystallographic properties.

4.2.1 X-Ray Diffraction (XRD)

To evaluate the structural characteristics of the grown Er doped samples, XRD measurements were performed using a PANalytical (EMPYREAN) X-ray diffractometer. The XRD patterns of Er doped GaN epilayer and Er doped AlN Epilayer are presented in figure 23 and 24, respectively, for comparison with that of MQWs:Er which is presented in figure 25. From the XRD patterns of the GaN:Er in figure 23, the sharp and clear peaks seen for both structures reveals crystalline nature of both structures. The characteristic peak of the (002) plane of GaN can be seen at $2\theta = 34.56°$ [32]. The pattern shows another pattern at the angle $2\theta \approx 74°$ which is related to the

(004) plane of GaN as it can be seen in the figure. The c-plane single crystal sapphire substrate also exhibits two peaks as apparent in the diffractogram, these are the (006) plane at 41.67° and the (012) plane at nearly 92°. This XRD pattern concludes that the GaN:Er sample has a c-plane Wurtzite structure and that it has a crystalline nature confirmed by the absence of any other peaks.

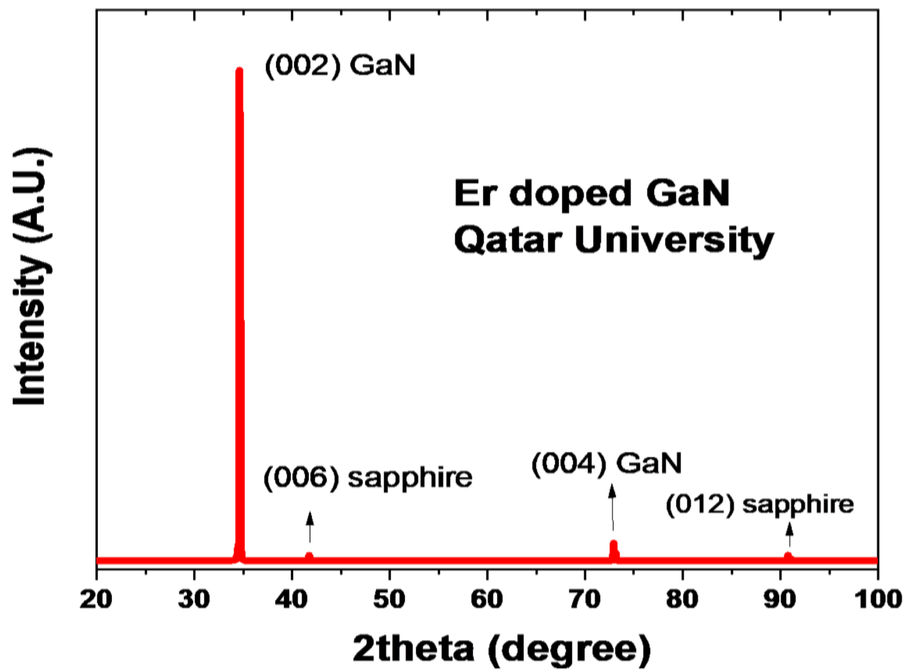

Figure 23: XRD patterns of GaN:Er epilayer.

Coming to the AlN:Er epilayer shown in figure 24, 4 peaks are seen in the obtained XRD pattern. AlN's (002) and (004) planes are detected at $2\theta \approx 36°$[46] and $2\theta \approx 76°$, respectively. The presence of these peaks ones again indicated that the AlN epilayer is crystalline in nature. The sapphire substrate once again was apparent at $2\theta = 41.67°$ resulting from the (006) plane and the (012) plane at around $2\theta = 92°$.

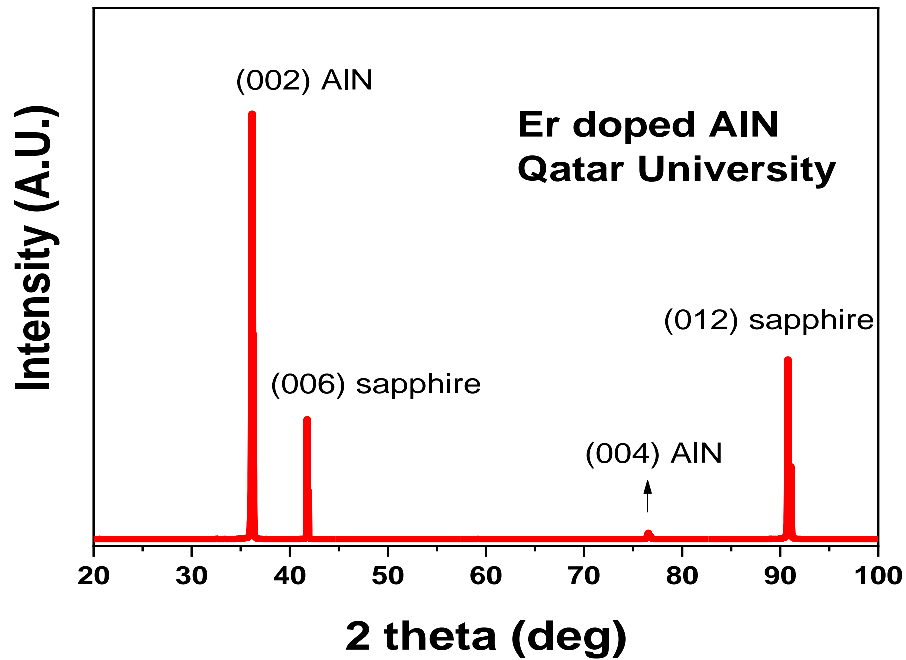

Figure 24: XRD pattern of AlN:Er epilayer grown on sapphire.

The performed XRD study on the MQWs:Er provided information about the quality of the interface between the wells and barriers of the structure. As figure 25 shows, the labeled peak at 2θ =36° coming from the (002) plane of AlN layers in the MQWs structure while the satellite peaks originated from the Er doped AlN/GaN MQWs. The distinct satellite peaks showing in the diffraction patterns indicates that the interfaces between wells and barriers are highly defined and clear, which is an important asset to achieve the maximum quantum confinement possible[8].

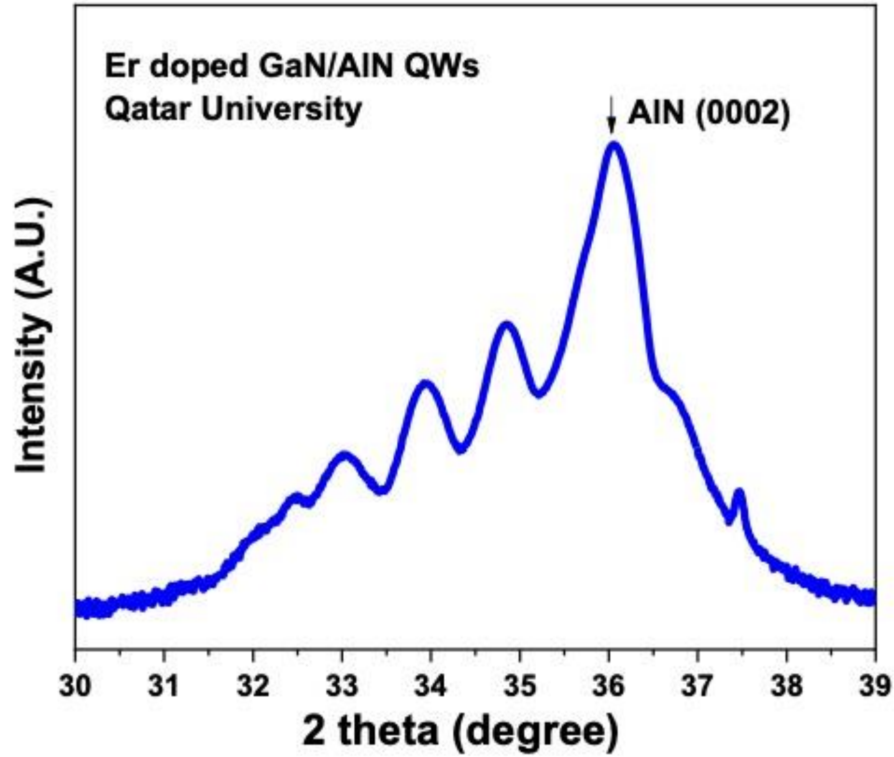

Figure 25: XRD pattern of Er Doped AlN/GaN MQWs

Using the (002) planes of AlN and GaN and their relative theta's, the lattice parameters c and the interplanar spacing (d_{hkl}) for their hexagonal structure, can be calculated using Bragg's law in Equation (3-1).

For AlN at (36°):

$$n\lambda = 2d_{hkl}sin\theta$$

with, n =1, λ = 0.154 nm. d_{hkl} is the interplaner spacing of the crystal which can be calculated by the d-spacing equation number (3-2):

$$d_{hkl} = \frac{1}{\sqrt{\frac{4}{3}\left(\frac{h^2+hk+k^2}{a^2}\right)+\frac{l^2}{c^2}}}$$

and (hkl) are the miller indices (002). θ is the angle of incidence which is 36°/2=18°.

So, to solve equation (3-1) for d:

$$d_{hkl} = \frac{n\lambda}{2sin\theta} = \frac{1 \times 0.154}{2\sin(18)}$$

$$\boldsymbol{d_{hkl} = 0.2492\ nm = 2.49}\ \text{Å}$$

Now, given h=0, k=0, and l=2, solving the equation for c:

$$d_{hkl} = \frac{1}{\sqrt{\frac{4}{3}\left(\frac{h^2 + hk + k^2}{a^2}\right) + \frac{l^2}{c^2}}} = \frac{1}{\sqrt{\frac{l^2}{c^2}}} = \frac{1}{\frac{l}{c}} = \frac{c}{l}$$

$$\boldsymbol{c} = d_{hkl} \times l = 0.2492 \times 2 = \boldsymbol{0.4982 \cong 0.49\ nm}$$

For GaN at (34.56°):

$$n\lambda = 2d_{hkl}sin\theta$$

with, n =1, λ = 0.154 nm. d_{hkl} is the interplaner spacing of the crystal which can be calculated by equation (3-2)

$$d_{hkl} = \frac{1}{\sqrt{\frac{4}{3}\left(\frac{h^2 + hk + k^2}{a^2}\right) + \frac{l^2}{c^2}}}$$

and (hkl) are the miller indices (002). θ is the angle of incidence which is 34.56°/2=17.28°.

So to solve equation (3-1) for d:

$$d_{hkl} = \frac{n\lambda}{2sin\theta} = \frac{1 \times 0.154}{2\sin(17.28)}$$

$$\boldsymbol{d_{hkl} = 0.2592\ nm = 2.59}\ \text{Å}$$

Now, given h=0, k=0, and l=2, solving equation (3-2) for $\boldsymbol{c}$:

$$d_{hkl} = \frac{1}{\sqrt{\frac{4}{3}\left(\frac{h^2+hk+k^2}{a^2}\right)+\frac{l^2}{c^2}}} = \frac{1}{\sqrt{\frac{l^2}{c^2}}} = \frac{c}{l}$$

$$\boldsymbol{c} = d_{hkl} \times l = 0.2592 \times 2 = \mathbf{0.5184\ nm} \cong \mathbf{5.18}\ \text{Å}$$

The obtained d-spacing (d_{hkl}) and lattice parameter (c) agrees in value with what has been reported by B. Kuppulingam and Ross, respectively [47] [48].

4.2.2 Raman spectroscopy

Raman scattering measurements were performed on the MQWs:Er structure and on the GaN:Er and AlN:Er epilayers for comparison and referencing. GaN and AlN have very well-known and extensively studied Raman vibrational modes. The atomic displacements of the possible vibrational phonons of Wurtzite GaN are illustrated in Figure 26 which are : the Raman and infrared (IR) active modes A_1 and E_1 with longitudinal optical component (LO) and transverse optical components (TO) phonon frequencies, the Raman active E_2 mode in both (low and high) phonon frequencies and lastly the silent B_1 (low and high) phonons, the number between parentheses are the frequencies of these vibrations in THz [49].

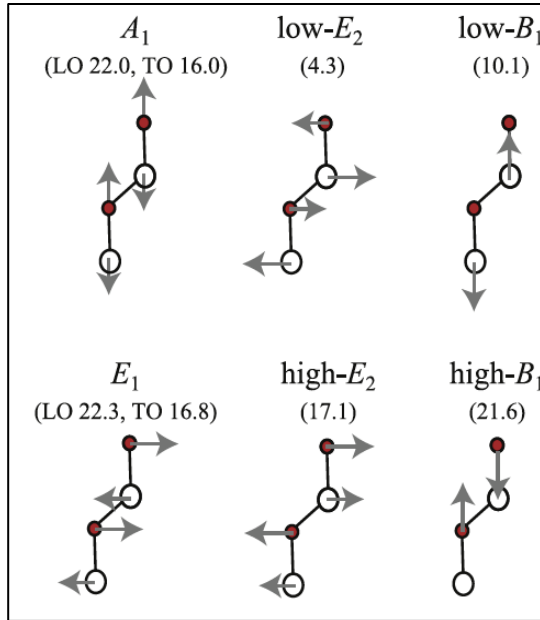

Figure 26: Different phonons and their relative atomic displacements in Wz GaN with Ga atoms colored white [49]*,*

Figure 27 shows the obtained Raman spectrum of the GaN:Er epilayer, two phonon modes were detected for GaN in addition to two other modes coming from the sapphire substrate. The first GaN related peak was observed at 572 cm^{-1} which was related to the strong E_2(high) phonon mode and the second peak was at 738 cm^{-1} related to the A_1(LO) mode. These results are comparable to data in literature such as a published study by Z. C. Feng et. al. were the phonon modes of MOCVD grown GaN layers E_2(high) and A_1(LO) were found at 567 cm^{-1} and 735 cm^{-1}, respectively. [50][51].

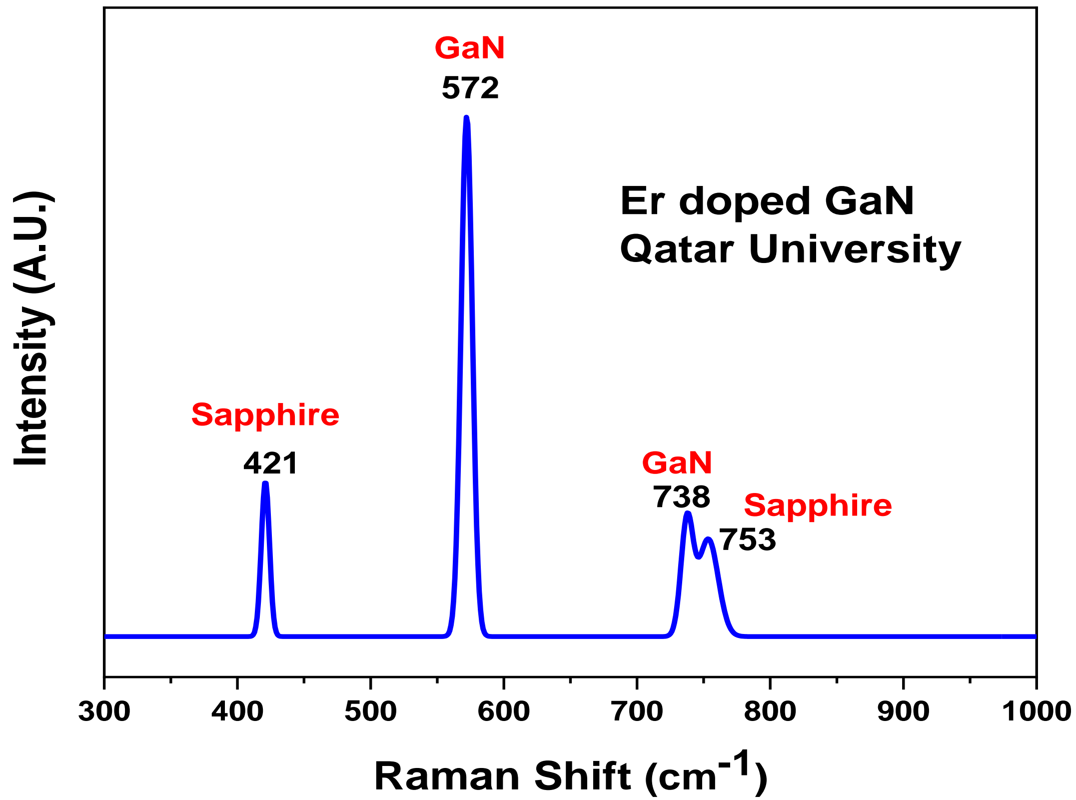

Figure 27: Raman shifts of GaN:Er epilayer.

The Raman spectrum AlN:Er epilayer shown in figure 28 exhibits two phonon modes for AlN, these are the E_2(high) and A_1(LO) at 661 cm^{-1} and 892 cm^{-1}, respectively [52]. Sapphire substrate also show strong signals in GaN:Er and AlN:Er epilayer at 421 cm^{-1} (shown only on GaN:Er graph) and 753 cm^{-1} related to the E_2(high) and A_1(LO) modes, respectively [53].

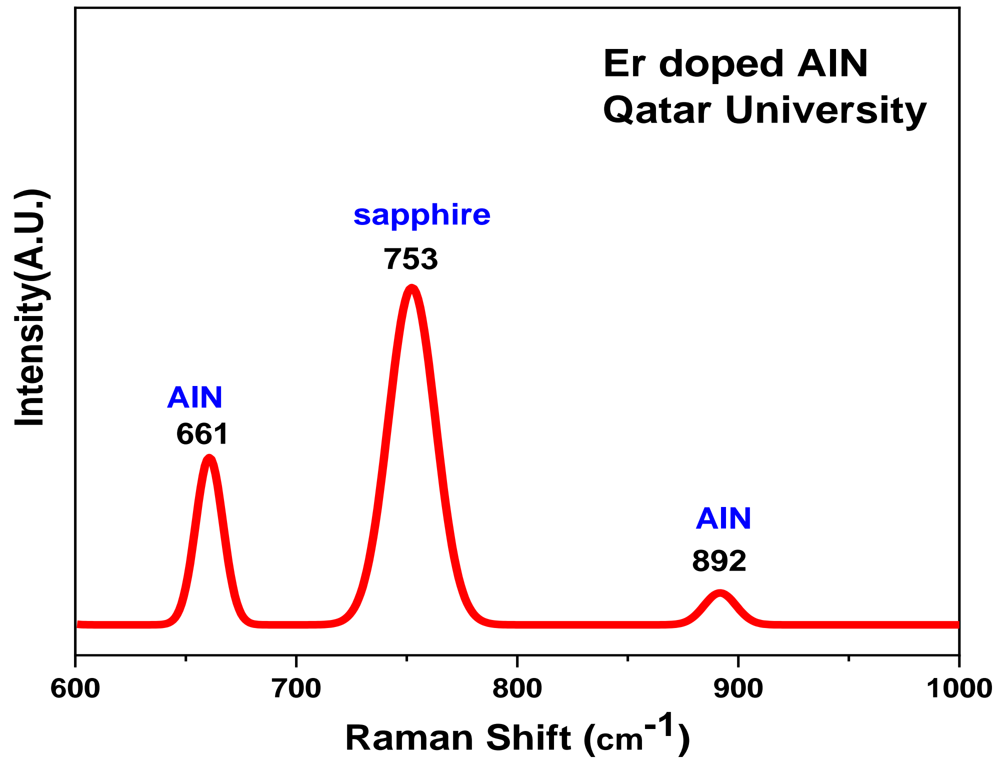

Figure 28: Raman shifts of AlN:Er epilayer.

When a polar semiconductor is in a superlattice or quantum well structure with another semiconductor having a different dielectric constant, it is a known fact that the interface phonon modes are a result of combined modes of both materials. Typically, the layered interfaces of nanostructures such as MQWs provide additional phonon modes These modes resulting from the nanostructured material usually have stronger frequencies than that of the bulk material. However, it is generally a complicated task to identify the phonon modes of structures such as superlattices and multiple quantum wells, due to structural alterations that happen along the z-axis during growth [54]. The association of each peak to its phonon mode for the AlN/GaN:Er MQWs understudy have been done by comparing to the above discussed epilayers and results from previous studies. As shown in figure 29, peaks seen at 596 cm^{-1} and 741 cm^{-1} are E_2(high) and A_1(LO) phonon modes of GaN well. A stress free GaN film

should have an E_2(high) mode at 567.6 according to [55]. Thus, the presence of a blue shift of 28.4 cm^{-1} postulates that the structure is under a compressive stress applied on the GaN well [54]. Phonon modes at 660 cm^{-1} and 892 cm^{-1} are both coming from the compressed AlN buffer layers and are related to the E_2(high) and A_1(LO) phonons, respectively. Furthermore, the AlN barrier is showing a phonon mode at 635 cm^{-1} representing the E_2(high) vibration and is red shifted below the unstressed value for this particular mode as a result of the increased tensile stress caused by the growing GaN well [55]. The peak at 421 cm^{-1} is related to the sapphire substrate as it has been mentioned previously [56].

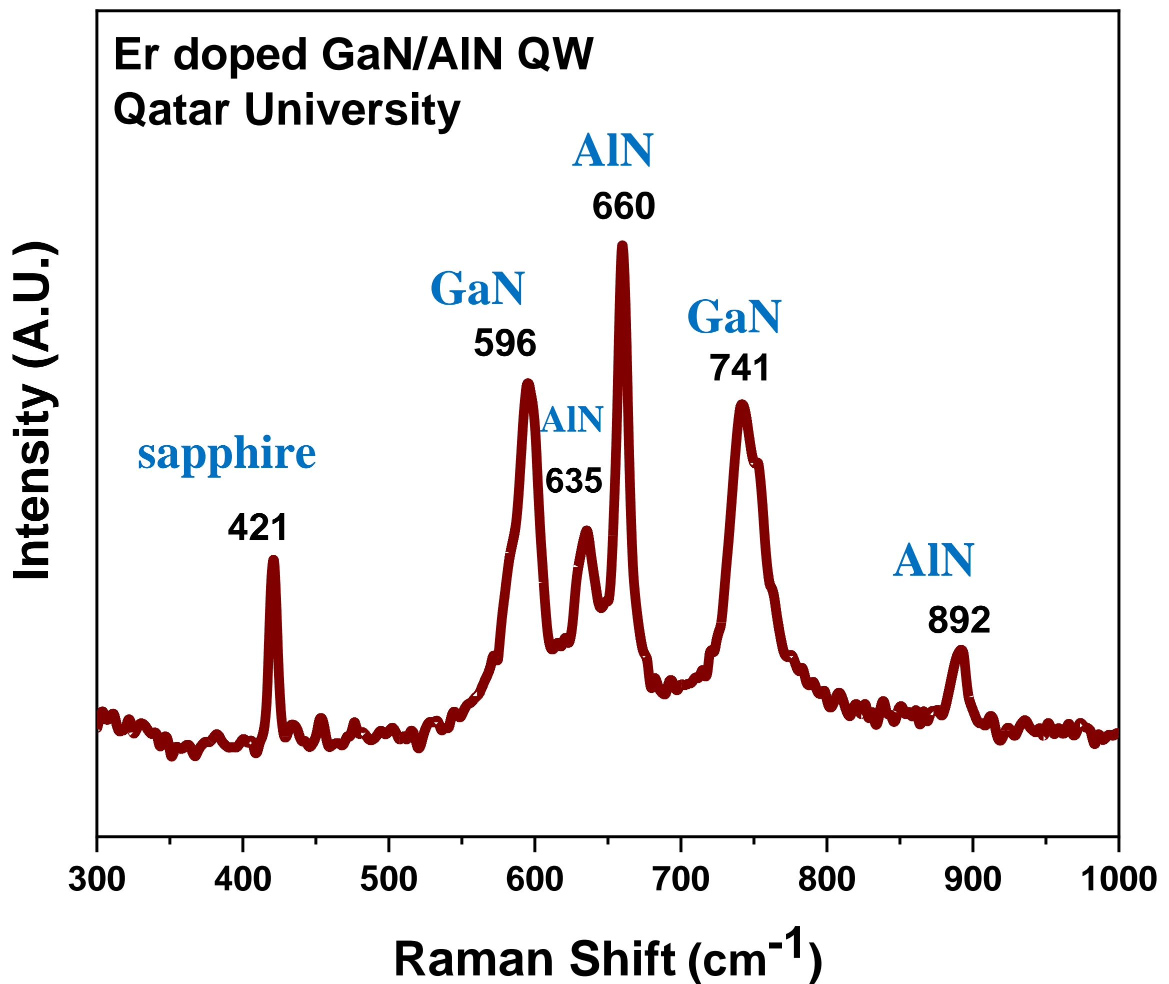

Figure 29: Raman shifts of AlN/GaN:Er MQWs.

4.3 Transmission electron microscopy (TEM)

The microstructure of the MQWs:Er was investigated using ThermoFisher Scientific TalosF200X TEM coupled with a SuperX EDS system. STEM micrographs were recorded with a High Annular Dark Field Detector. TEM images were acquired using BM-CETA 16M CCCD camera.

i. Scanning transmission electron microscopy (STEM)

STEM is a mode of TEM that allows taking scanning images of the surface morphology of samples. Since the structure of the MQWs is composed of layers and are far too thick for the electron beam of TEM to navigate through, the samples were first treated and prepared using Focused ion beam microscopy (FIB). FIB is a destructive technique that usually complements TEM and SEM machines, it uses a focused ion beam to chemically Etch the sample by sputtering the surface with these energetic ions leaving a very thin and sheer sample suitable for TEM imaging [57]. After being prepared, STEM images were taken for the MQWs:Er and are shown in figure 30. The layered structure of the grown MQWs:Er sample can be seen in figure 30(a), starting from the sapphire (Al_2O_3) substrate in the back, followed by the undoped AlN template and two buffer layers and finally the MQWs:Er structure . The 50 periods of the MQWs:Er can be clearly seen in figure 30(b) with sharp and distinctly clear interfaces between the undoped AlN barrier layers (dark) and the Er doped GaN wells (bright) shown in image 30(c). The thicknesses of the Er hosting GaN wells were measured by TEM to be 5.5 nm ± 0.3 nm which makes the total thickness of the Er doped layer (GaN:Er) to be around 250 nm. The AlN barrier's thickness was measured to be slightly higher than the GaN with a thickness of 6 nm and a ± 0.3 nm.

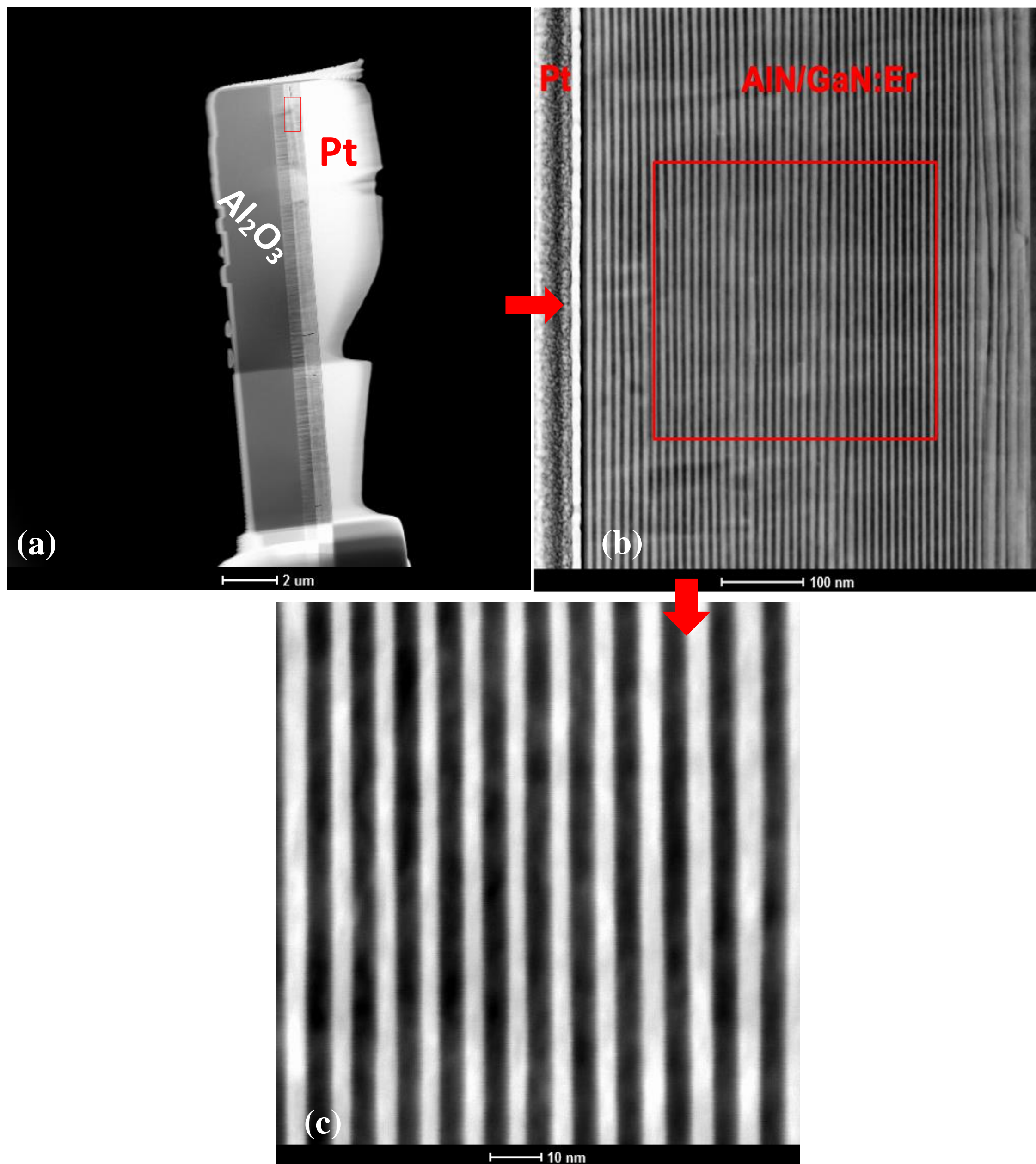

Figure 30: STEM images of MQWs:Er at different magnifications, bright strips are the GaN:Er Wells

ii. Interplanar spacing (d-Spacing)

d-spacing refers to the physical distance between atomic planes within the crystal lattice that gives rise to the various diffraction peaks seen in XRD diffractograms. Figure 31 bellow shows bright field TEM images of the lattice planes of the undoped AlN template in image (a) and the AlN/GaN:Er MQWs in

image (b). The measured d-spacing for AlN template area in image (a) and in the AlN barrier regions of image (b) showed a value of 0.49 nm which corresponds to the crystallographic plane (001) [58]. Additionally, the interplanar space between planes of GaN:Er shown in image (b) measured 0.518 nm which corresponds to the (004) plane[48].

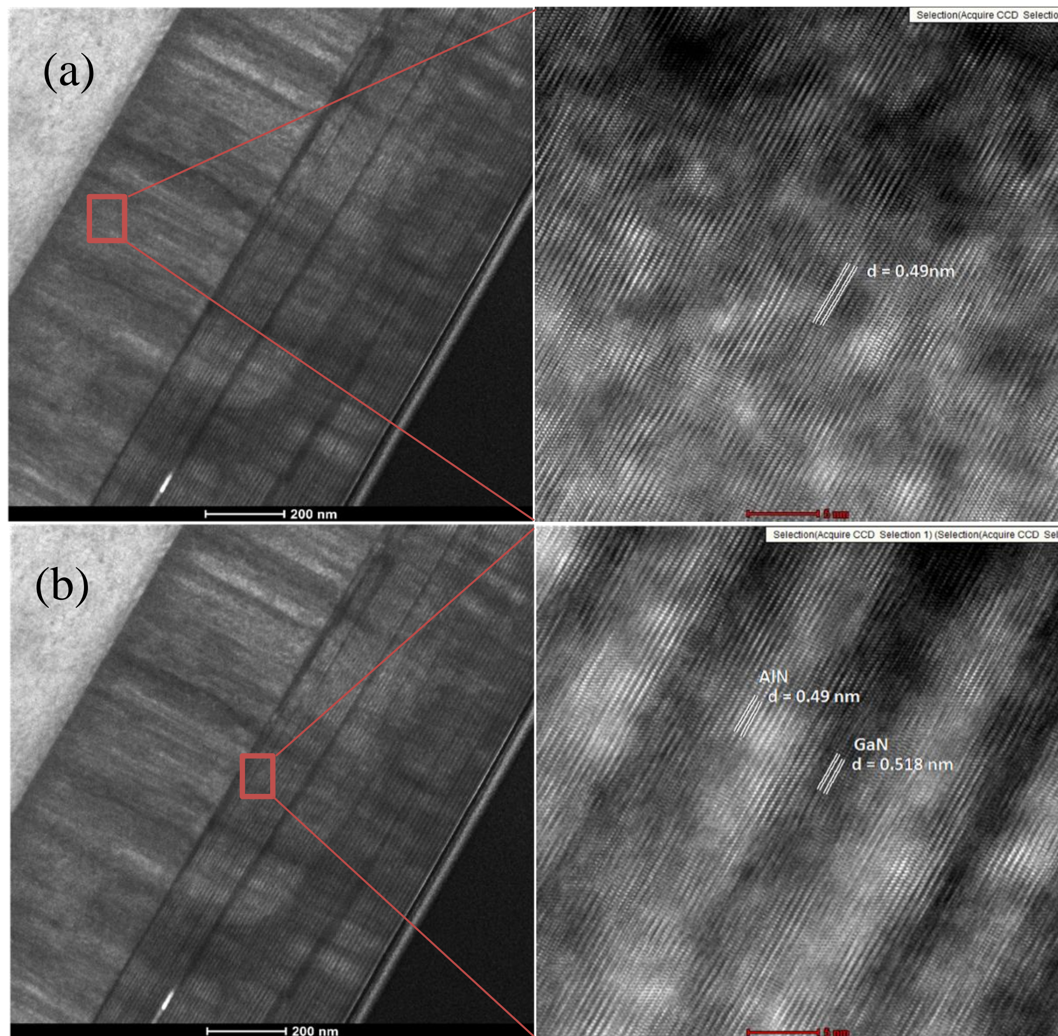

Figure 31: Bright field STEM showing Interplanar spacing in the undoped AlN tempelate(a) and AlN/GaN:Er quantum wells (b)

iii. Selected Area Electron Diffraction (SAED) pattern.

SAED is a crystallographic technique that gives information about the crystal structure and the d-spacing. Figure 32 shows the shows the selected area diffraction pattern (SADP) of the MQWs:Er structure with a diffraction patterns (DP) for the undoped AlN template on top and a diffraction pattern for the MQWs structure on the bottom. Since it is a known fact that single crystals show up as arrays of discrete spots in the DP as a result of the highly ordered atoms within the single crystal, while polycrystalline materials which are in fact many single crystals joined together, the numerous amount of crystals reflect electrons in a matter that shows the discrete spots as rings [59]. This indicates that the deposited un-doped AlN template layer is a single crystalline layer because of the apparent spot patterns. The same conclusion applies to the AlN/GaN:Er layers were the DP shows arrays of discrete spots. However, as shown in figure 32, the spots in the MQWs area are not as sharp and round as the spots in the undoped AlN layer, they rather resemble stretched out spots or small rods. This elongation of the lattice points is for the sample being thin in the reciprocal direction corresponding to the real-space direction in which the sample is thin [60]. A very useful outcome of SAED, in addition to the ability to decide on the crystalline nature, is the capacity to directly measure the d-spacing between lattice planes, and the ability to index each spot. The measured interplanar distance in the top DP of the AlN template layer shown in figure 35 are 0.49 nm which corresponds to the d-spacing of the (001) plane, while the 0.26 nm interplanar spacing corresponds to the (100) plane [58].

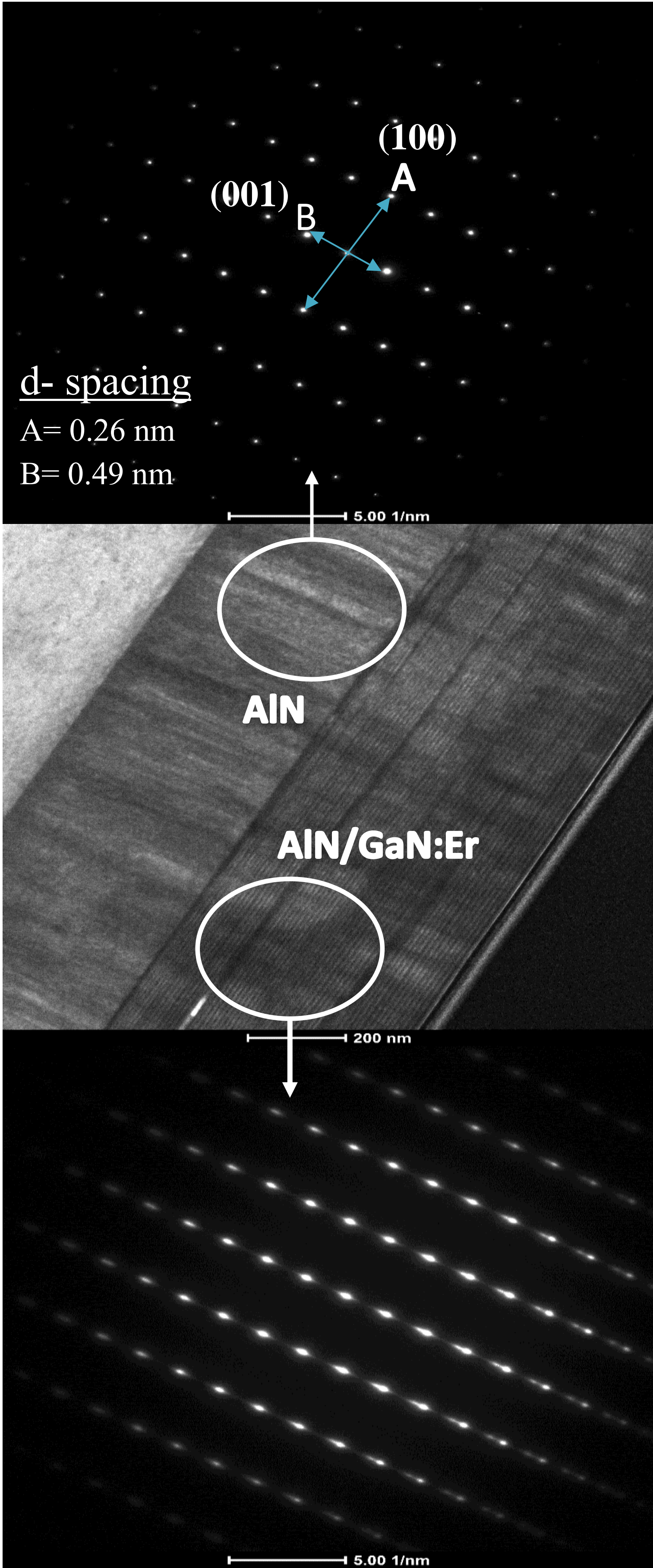

Figure 32: SAED patterns for the undoped AlN buffer layer (Top) and the AlN/GaN:Er Quantum well structure (Bottom).

iv. Elemental mapping using Energy dispersive spectroscopy (EDS)

The importance of elemental mapping for this study is in its ability to show the distribution of Al, Ga, and N within the structure. Visualizing the distribution of these elements will further confirm the targeted structure of a quantum well and provide an assessment to the quality of growth. EDS mapping of the MQWs:Er done using High-Angle Annular Dark-Field imaging (HAADF). This technique is a method of STEM that has a very high image resolution and is highly sensitive to variations in the atomic number (Z) of atoms within the sample, producing an annular dark-field image [61]. In a HAADF-STEM dark field image, the element with a higher Z number will cause more electrons to be scattered at high angles due to higher electrostatic interactions between the nucleus and the electron beam of the TEM, this will result in the HAADF detector to sense more signals from the higher Z atoms, which causes these atoms to appear in brighter shades in the final image.

The EDS images in Figure 33 show the distinctive structure of a quantum well, with abrupt interfaces between barriers and wells. The elemental mapping done at high resolution (20 nm), shows Al in the dark areas whereas Ga is located in brighter areas with no interference between the layers of the MQWs. Nitrogen can be seen to be evenly distributed throughout the structure.

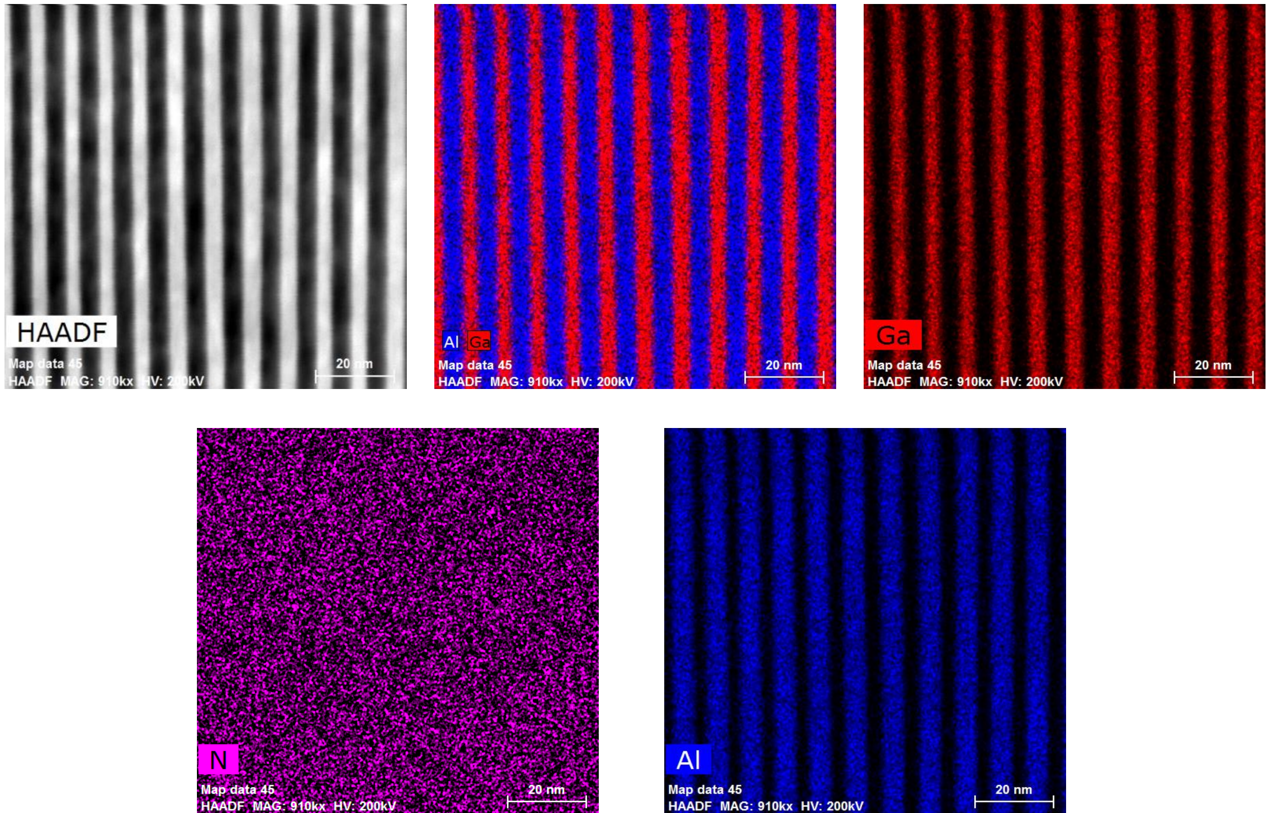

Figure 33: Energy dispersive spectroscopy elemental scanning of MQW:Er done using HAADF imaging.

When it comes to detection of dopants within semiconductor nanomaterials, today, state-of-the art TEM/EDS machines are limited to very few elements, namely phosphorus and arsenic, in very few hosts such as Si and SiGe with detection limits that cannot go below 10^{20} atoms/cm^3. Detection of lower quantities of dopants requires specific settings and qualities of the used EDS/TEM device such as using very low voltage and specific hardware which was not available for this study [62]. Thus, due to limits in its detection ability, the doping of Erbium within the GaN well layers wasn't detected by EDS, which was an expected outcome because the concentration of Er is below the detection limit, that's why it was necessary to use another method to detect the presence of Er in the MQW structure and GaN layers specifically.

4.4 Surface Analysis: Time-of-Flight Secondary Ion mass spectroscopy (ToF-SIMS)

As mentioned before, the Er concentration in the quantum well structure was below the minimum detection limit of EDS so it wasn't seen in the elemental scanning of samples. To overcome this issue and to confirm the doping of the GaN by Er^{3+}, ToF-SIMS was used. ToF-SIMS is a powerful tool for detecting elements and compounds in the parts per million (ppm) and parts per billion (ppb) range, the tool used for this test is an IonTOF ToF-SIMS 5-100. This system used a Bismuth primary source at 30kV voltage and 28 nA ion current. The sputtering source was O_2 at 2 kV providing 610 nA ion current. The ToF-SIMS profile of the MQWs:Er is shown in figure 34**,** where the signals of Al^+, Ga^+, and Er^{3+} are showing in a sinusoidal wave manner. An Alternation of the wave's crests (maximum amplitude point) of Al^+ and Ga^+ is seen, meaning that whenever a crest exists for one element's signal, a trough (minimum amplitude point) of the other element is seen at the exact point in the x-axis direction as it is denoted by the vertical dashed line. This means that when a high signal of Ga is detected, a low signal of Al is seen simultaneously, and vice versa. This is an indication of the presence of alternating layers in the structure and a characteristic of the multiple quantum wells configuration.

The signal of Er is detected by ToF-SIMS and it is following that of Ga^+, which is a direct sign that Er^{3+} ions are imbedded within the GaN well layers only. The wave cycle of Ga^+ signal (time between two successive crests or troughs) is almost fixed at around 112 seconds, which could be an indication for the uniformity of the thicknesses of each GaN:Er well layer detected throughout the testing period. Same thing applied to the wave cycle of Al^+ signal.

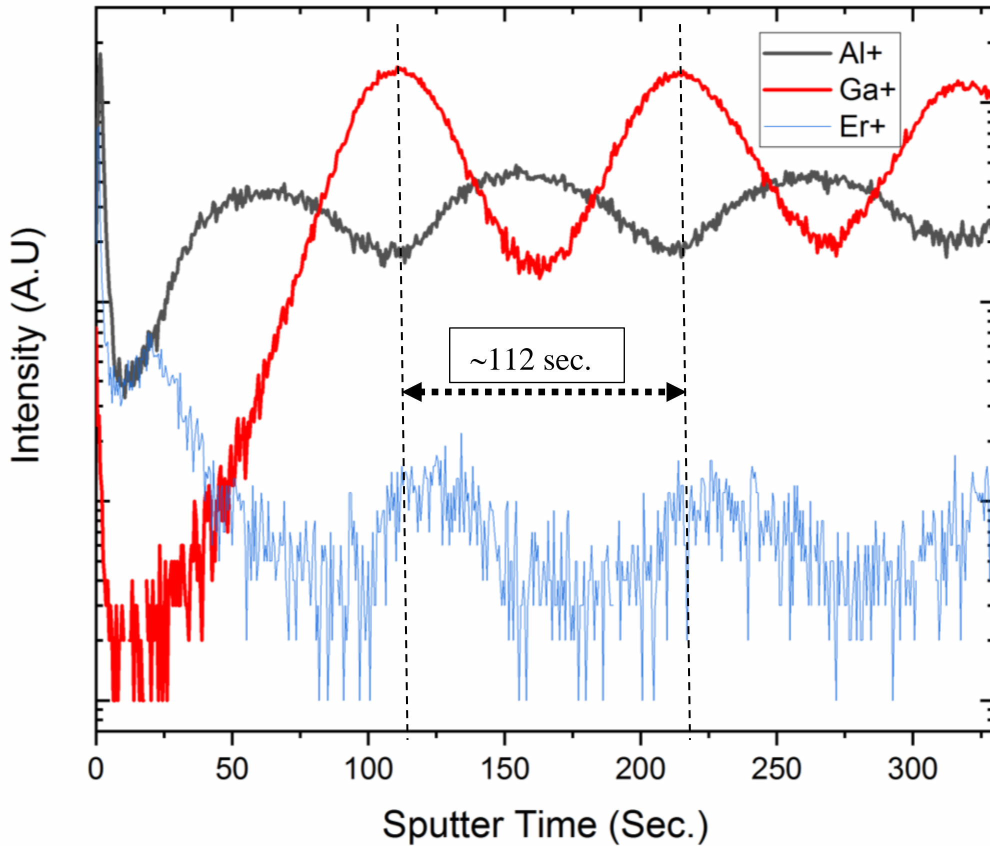

Figure 34: ToF-SIMS profile of MQWs:Er showing Er^{+}, Ga^{+} and Al^{+} on a log scale y-axis.

4.5 Optical properties: Photoluminescence spectroscopy.

As we've established before, our core interest is to examine the effect of incorporating the Er ions in a multiple quantum well environment on the PL intensity of the Er^{3+} transition from energy level $^4I_{13/2}$ to energy level $^4I_{15/2}$. This transition will produce a characteristic PL emission at 1.54 µm. PL measurements were performed on GaN:Er epilayer, AlN:Er epilayer, and AlN/GaN:Er MQWs and the results are shown in figures 35-37 below. Both GaN:Er (figure 35) and AlN:Er (figure 36) exhibited an emission peak at 1.54 µm. The PL intensity of the 1.54 µm emission was found to be slightly higher for the AlN:Er epilayer compared to GaN:Er. This could be explained by the better thermal stability of AlN and also because of the thermal quenching effect on the PL intensity of GaN:Er at room temperature [63]. The PL spectrum of the

MQWs:Er in figure 37 shows a significant increase in the PL intensity at 1.54 µm, the intensity is almost 10 times higher than that of GaN:Er epilayer putting in mind the similar Er active layer thickness and equivalent Er concentration. The strong increase in the PL intensity is a direct indication that Er^{3+} optical centers were efficiently excited due to the increased density of charge carriers, meaning that proper quantum confinement of carriers has been achieved by using this MQW structure which led to increased overall quantum efficiency for the IR emission at 1.54µm.

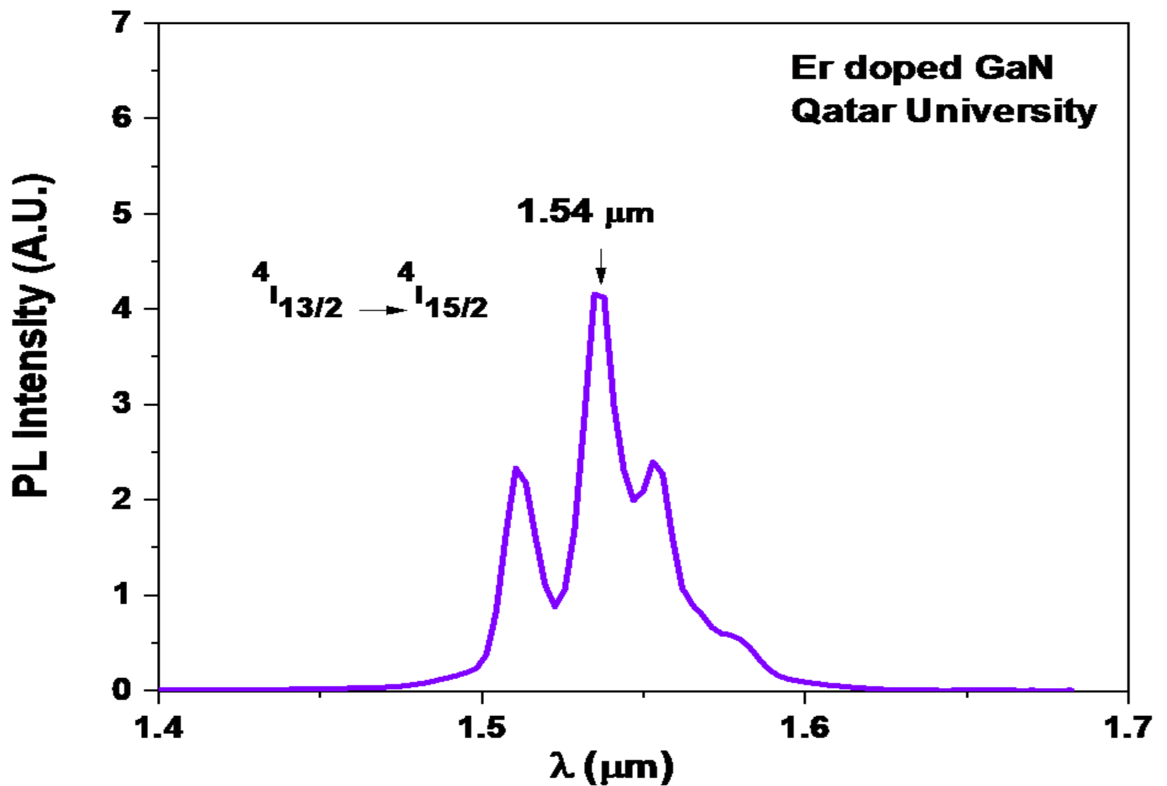

Figure 35: PL spectrum of GaN:Er Epilayer

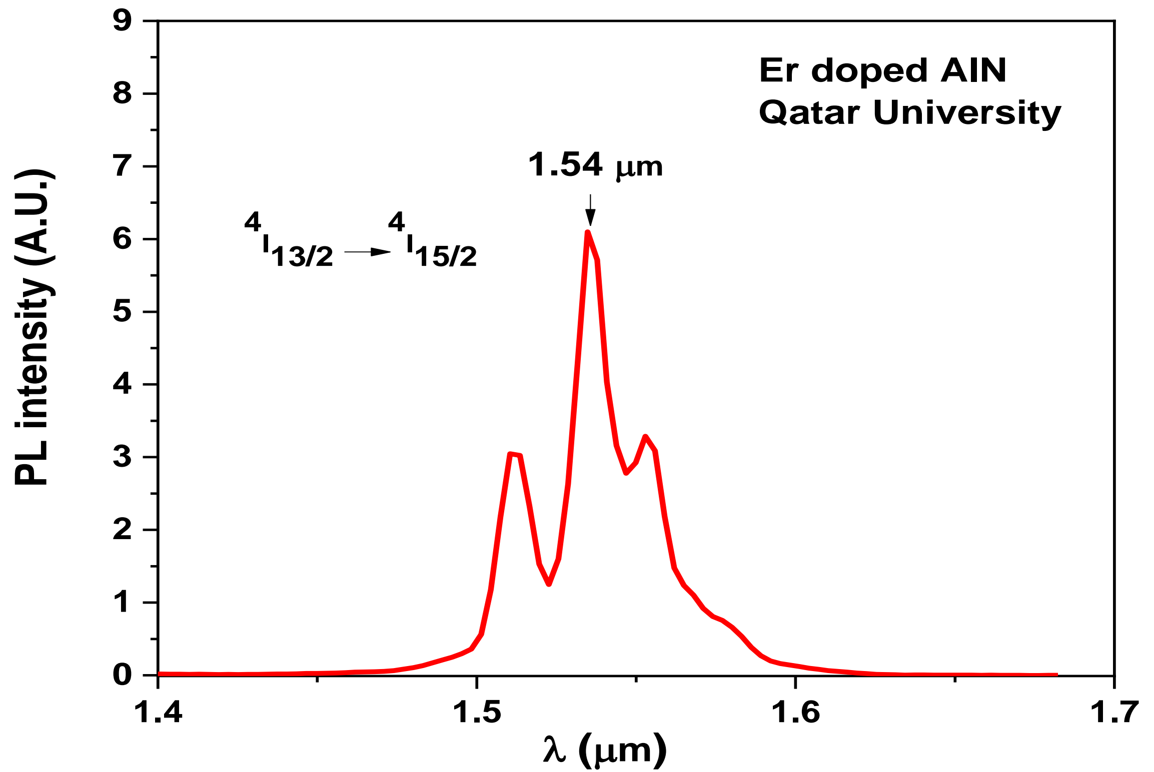

Figure 36: PL spectrum of AlN:Er epilayer

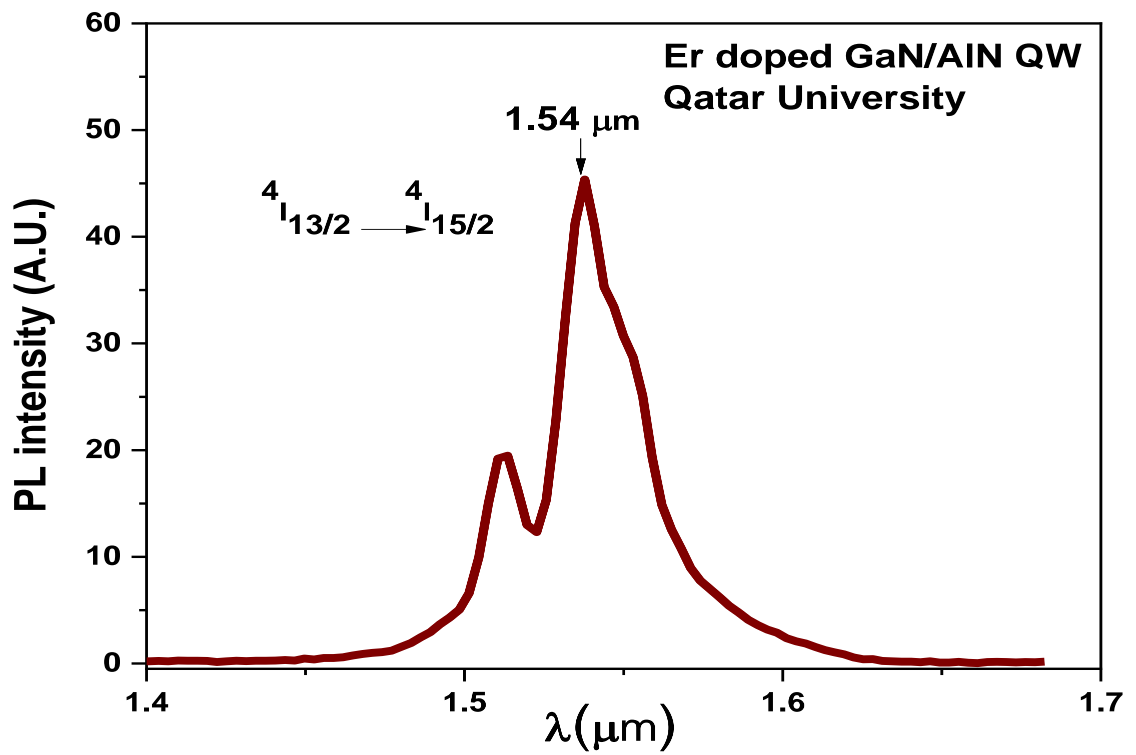

Figure 37: PL spectrum of AlN/GaN:Er MQWs.

CHAPTER 5: CONCLUSION

Er-doped AlN/GaN Multiple Quantum well structures composed of 50 periods were grown by means of metalorganic chemical vapor deposition in quest to enhance the emission intensity of Er^{3+} ions embedded within the GaN well layers. The Er^{3+} active layer in the MQWs was about 250 nm in thickness, two comparable epilayers of GaN:Er and AlN:Er were grown using the same method and used as a reference for comparison. X-ray diffraction showed a single crystallinity diffraction patterns, with the characteristic peaks of GaN and AlN at their respective diffraction angles. XRD also concluded that the interfaces between barriers and wells are of high quality because distinct satellite peaks were seen. The characteristic phonon modes of AlN and GaN were investigated and detected by Raman spectroscopy, then, results were compared to the Raman peaks resulting from the MQWs. Slight shifts were seen in the phonon frequencies resulting from the built up compressive and tensile stresses acting on GaN:Er and AlN:Er layers ,respectively. The nanostructure of the grown MQWs was investigated by STEM and coupled EDS system. Clean and sharp interfaces between barriers and wells indicated a high-quality growth system and method, with a measured thickness of around 5.5 nm for the GaN wells and 6 nm for the AlN barriers with minimum variations. STEM imaging was also used to measure the interplanar spacing of the GaN and AlN layers. EDS images showed the elemental distribution of Ga, Al and N within the structure. Additionally, the studied diffraction patterns of the undoped AlN layer and the MQWs confirmed the high crystal quality of the MOCVD grown MQW structure. ToF-SIMS measurements confirmed the MQWs structure from the sinusoidal shape of the graph, and also detected the presence of Er, which was below detection limit of the EDS system. Finally, PL measurements were done to evaluate the effect of using the MQWs structure on the characteristic IR emission of Er^{3+} ions at

1.54 μm . Compared to the GaN epilayer, AlN/GaN:Er multiple quantum wells showed a PL emission intensity almost 10 times higher than that of GaN:Er epilayer, mainly due to the achievement of efficient carrier confinement. In Conclusion, this study showed that the application of MQWs structures as hosts for the Er^{3+} ions significantly increases the quantum efficiency of the 1.54 μm emission compared to GaN:Er epilayers, which makes them a promising technology for applications in optoelectronic devices generally, and in optical fiber communications specially.

Future plans

The use of MQWs structure as hosts for the Er ions was recognized to amplify the PL emission intensity at 1.54 μm. Further work could be done to achieve even better emissions by optimizing the growth parameters of the MQWs different layers to achieve more easier, efficient and economic growth methodology that can result in more uniform thickness of layers, enhanced crystallinity and morphological properties leading to better quantum confinement performance. Which will ultimately be contributing in the manufacturing of better performing optoelectronic devices.

REFERENCES

[1] P. Pampili and P. J. Parbrook, "Doping of III-nitride materials," *Mater. Sci. Semicond. Process.*, vol. 62, no. October 2016, pp. 180–191, 2017.

[2] B. Monemar and G. Pozina, "Group III-nitride based hetero and quantum structures," vol. 24, pp. 239–290, 2000.

[3] M. T. Hardy, D. F. Feezell, S. P. Denbaars, and S. Nakamura, "Group III-nitride lasers," *Mater. Today*, vol. 14, no. 9, pp. 408–415, 2011.

[4] S. N. Mohammad, "PROGRESS AND PROSPECTS OF GROUP-III SEMICONDUCTORS," vol. 20, no. 516, pp. 361–525, 1996.

[5] I. Bhat, *Physical properties of gallium nitride and related III–V nitrides*. Elsevier Ltd, 2019.

[6] C. Ugolini, N. Nepal, J. Y. Lin, H. X. Jiang, and J. M. Zavada, "Excitation dynamics of the 1.54 μm emission in Er doped GaN synthesized by metal organic chemical vapor deposition," *Appl. Phys. Lett.*, vol. 90, no. 5, pp. 2005–2008, 2007.

[7] T. Mohammed, A. Tahtamouni, X. Du, J. Lin, and H. Jiang, "Erbium-doped AlN epilayers synthesized by metal-organic chemical vapor deposition," vol. 5, no. 3, pp. 284–286, 2015.

[8] T. M. Al tahtamouni, M. Stachowicz, J. Li, J. Y. Lin, and H. X. Jiang, " Dramatic enhancement of 1.54 μ m emission in Er doped GaN quantum well structures ," *Appl. Phys. Lett.*, vol. 106, no. 12, p. 121106, 2015.

[9] L. J. Mawst and N. Tansu, "5.15 - Quantum-Well Lasers and Their Applications," P. Bhattacharya, R. Fornari, and H. B. T.-C. S. S. and T.

Kamimura, Eds. Amsterdam: Elsevier, 2011, pp. 626–682.

[10] R. J. Martín-Palma and J. M. Martínez-Duart, “Chapter 5 - Semiconductor Quantum Nanostructures, Multiple Quantum Wells, and Superlattices,” in *Nanophotonics*, R. J. Martín-Palma and J. M. B. T.-N. for M. and P. (Second E. Martínez-Duart, Eds. Elsevier, 2017, pp. 107–131.

[11] H. Morkoç, “Aluminum, Gallium, and Indium Nitrides,” *Encycl. Mater. Sci. Technol.*, pp. 121–126, 2001.

[12] S. Pimputkar, *Gallium nitride*. Elsevier Ltd, 2019.

[13] H. P. Maruska and J. J. Tietjen, “The preparation and properties of vapor-deposited single-crystal-line GaN,” *Appl. Phys. Lett.*, vol. 15, no. 10, pp. 327–329, 1969.

[14] S. Nakamura, “GaN growth using GaN buffer Layer,” pp. L1705–L1707, 1991.

[15] V. Vechten, “Gallium Nitride, Bulk,” 2000.

[16] M. Hatanaka and S. Yabushita, “Theoretical study on the f-f transition intensities of lanthanide trihalide systems,” *J. Phys. Chem. A*, vol. 113, no. 45, pp. 12615–12625, 2009.

[17] U. de C. Braud, Alain (Centre de Recherche sur les Ions, les Matériaux et la Photonique (CIMAP), “Excitation Mechanisms of RE Ions in Semiconductors,” in *Rare Earth Doped III-Nitrides for Optoelectronic and Spintronic Applications*, Springer, Dordrecht, pp. 270–307.

[18] R. Lavi *et al.*, “Efficient pumping scheme for neodymium-doped materials by direct excitation of the upper lasing level,” *Appl. Opt.*, vol. 38, no. 36, p. 7382, 1999.

[19] D. Sangta, F. Balembois, and P. Georges, “Nd:yag laser diode-pumped directly into the emitting level at 938 nm,” *CLEO/Europe - EQEC 2009 - Eur. Conf.*

Lasers Electro-Optics Eur. Quantum Electron. Conf., vol. 17, no. 12, pp. 10091–10097, 2009.

[20] H. J. Lozykowski, "Kinetics of luminescence of isoelectronic rare-earth ions in III-V semiconductors," *Phys. Rev. B*, vol. 48, no. 24, pp. 17758–17769, 1993.

[21] G. . Dieke, "Spectra and Energy Levels of Rare Earth Ions in Crystals," *Am. Inst. Phys. Handb.*, 1968.

[22] K. Ogasawara *et al.*, " Calculations of Complete 4 f n and 4 f n -1 5 d 1 Energy Level Schemes of Free Trivalent Rare-Earth Ions ," *Jpn. J. Appl. Phys.*, vol. 43, no. No. 5A, pp. L611–L613, 2004.

[23] B. Mitchell, *7 – MOCVD growth of Er-doped III-N and optical-magnetic characterization*. Elsevier, 2016.

[24] V. X. Ho, H. X. Jiang, J. Y. Lin, J. M. Zavada, and N. Q. Vinh, "Room-Temperature Lasing Action in GaN Quantum Wells in the Infrared 1.5 μ m Region," no. 001, 2018.

[25] T. M. A. L. Tahtamouni, J. Y. L. In, and H. X. J. Iang, "Current injection 1.54 μm light-emitting devices based on Er-doped GaN/AlGaN multiple quantum wells," vol. 6, no. 11, pp. 3476–3481, 2016.

[26] R. G. Wilson *et al.*, "1.54 um photoluminescence from Er implanted GaN and AlN," vol. 992, pp. 51–54, 1994.

[27] A. Polman, G. N. Van Den Hoven, J. S. Custer, J. H. Shin, R. Serna, and P. F. A. Alkemade, "Erbium in crystal silicon: Optical activation, excitation, and concentration limits," *J. Appl. Phys.*, vol. 77, no. 3, pp. 1256–1262, 1995.

[28] R. Dahal *et al.*, "Erbium-doped GaN optical amplifiers operating at 1 . 54 μ m," vol. 111109, no. 2009, pp. 3–6, 2014.

[29] P. N. Favennec, H. L'haridon, M. Salvi, D. Moutonnet, and Y. le Guillou,

"Luminescence of Erbium Implanted in Various Semiconductors: IV, III-V and II-VI Materials," *Electron. Lett.*, vol. 25, no. 11, pp. 718–719, 1989.

[30] J. Yin *et al.*, "Comparative spectroscopic studies of MOCVD grown AlN films on Al2O3 and 6H–SiC," *J. Alloys Compd.*, vol. 857, p. 157487, 2021.

[31] M. Nemoz, R. Dagher, S. Matta, A. Michon, P. Vennéguès, and J. Brault, "Dislocation densities reduction in MBE-grown AlN thin films by high-temperature annealing," *J. Cryst. Growth*, vol. 461, no. December 2016, pp. 10–15, 2017.

[32] E. Schilirò *et al.*, "Structural and electrical properties of AlN thin films on GaN substrates grown by plasma enhanced-Atomic Layer Deposition," *Mater. Sci. Semicond. Process.*, vol. 97, no. November 2018, pp. 35–39, 2019.

[33] X. Wang and A. Yoshikawa, "Molecular beam epitaxy growth of GaN , AlN and InN," vol. 49, pp. 1–33, 2004.

[34] L. Liu and J. H. Edgar, "Substrates for gallium nitride epitaxy," *Mater. Sci. Eng. R 37*, pp. 61–127, 2002.

[35] H. Rinnert, S. S. Hussain, V. Brien, J. Legrand, and P. Pigeat, "Photoluminescence properties of Er-doped AlN films prepared by magnetron sputtering," *J. Lumin.*, vol. 132, no. 9, pp. 2367–2370, 2012.

[36] H. Jiang, J. Lin, C. Ugolini, and J. Zavada, "ER DOPED III-NITRIDE MATERIALS AND DEVICES SYNTHESIZED BY MOCVD," 12/375,187, 2010.

[37] Y. B. Band and Y. Avishai, *Low-Dimensional Quantum Systems*. 2013.

[38] J. Wang, *Chemical Vapor Deposition and Its Applications in Inorganic Synthesis*. Elsevier B.V., 2017.

[39] L. Bergman and R. J. Nemanich, "RAMAN SPECTROSCOPY FOR

CHARACTERIZATION OF HARD , WIDE-BAND GAP SEMICONDUCTORS : Diamon, GaN, GaAlN, AlN,BN,” *Annu. Rev. Mater. Res.*, 1996.

[40] A. Benninghoven, “Chemical Analysis of Inorganic and Organic Surfaces and Thin Films by Static Time-of-Flight Secondary Ion Mass Spectrometry (TOF-SIMS).”

[41] C. Y. Tang and Z. Yang, *Transmission Electron Microscopy (TEM)*. Elsevier B.V., 2017.

[42] T. Walther, *Chapter 4 - Transmission Electron Microscopy of Nanostructures*. Elsevier Inc., 2017.

[43] B. J. Inkson, *2 - Scanning electron microscopy (SEM) and transmission electron microscopy (TEM) for materials characterization*. Elsevier Ltd, 2016.

[44] D. R. Baer and S. Thevuthasan, *Characterization of Thin Films and Coatings*, Third Edit. Elsevier Ltd., 2010.

[45] N. Patel, “Basic principle, Working and Instrmentation of Experimental techniques,” *Sardar Patel Univ.*, pp. 58–101, 2015.

[46] M. Bosund *et al.*, “Properties of AlN grown by plasma enhanced atomic layer deposition,” *Appl. Surf. Sci.*, vol. 257, no. 17, pp. 7827–7830, 2011.

[47] B. Kuppulingam, S. Singh, and K. Baskar, “Self-catalytic growth of AlN microrods on sapphire substrate,” *J. Cryst. Growth*, vol. 468, no. February 2020, pp. 856–861, 2017.

[48] J. Ross, M. Rubin, and T. K. Gustafson, “Single crystal wurtzite GaN on (111) GaAs with AIN buffer layers grown by reactive magnetron sputter deposition,” *J. Mater. Res.*, vol. 8, no. 10, pp. 2613–2616, 1993.

[49] K. Ishioka, K. Kato, N. Ohashi, H. Haneda, M. Kitajima, and H. Petek, “The effect of n- and p-type doping on coherent phonons in GaN,” *J. Phys. Condens. Matter*, vol. 25, no. 20, 2013.

[50] Z. C. Feng, M. Schurman, R. A. Stall, M. Pavlosky, and A. Whitley, “Raman scattering as a characterization tool for epitaxial GaN thin films grown on sapphire by turbo disk metal-organic chemical vapor deposition,” vol. 36, no. 13, pp. 2917–2922, 1997.

[51] K. Sarkar *et al.*, “Superlattices and Microstructures Raman analysis of phonon modes in a short period AlN / GaN superlattice,” *Superlattices Microstruct.*, vol. 115, pp. 116–122, 2018.

[52] V. Y. Davydov, Y. E. Kitaev, I. N. Goncharuk, and A. N. Smirnov, “Phonon dispersion and Raman scattering in hexagonal GaN and AlN,” vol. 58, no. 19, 1998.

[53] F. D. Cortes-Vega, W. Yang, J. Zarate-Medina, S. R. Brankovic, J. M. Herrera Ramírez, and F. C. Robles Hernandez, “Room-temperature synthesis of χ-Al2O3 and ruby (α-Cr:Al2O3),” *CrystEngComm*, vol. 20, no. 25, pp. 3505–3511, 2018.

[54] V. Darakchieva *et al.*, “Phonon mode behavior in strained wurtzite AlN/GaN superlattices,” *Phys. Rev. B - Condens. Matter Mater. Phys.*, vol. 71, no. 11, pp. 1–9, 2005.

[55] A. R. Goñi, H. Siegle, C. Thomsen, K. Syassen, and J. M. Wagner, “Effect of pressure on optical phonon modes and transverse effective charges in (formula presented) and (formula presented),” *Phys. Rev. B - Condens. Matter Mater. Phys.*, vol. 64, no. 3, pp. 1–6, 2001.

[56] D. Kirillov, H. Lee, and J. S. Harris, “Raman scattering study of GaN films,” *J. Appl. Phys.*, vol. 80, no. 7, pp. 4058–4062, 1996.

[57] J. L. Lue, T. F. Chang, J. C. Chen, and T. Wang, "A method for precise TEM sample preparation using the FIB ex-situ lift-out technique with a modified copper ring in semiconductor devices," *AIP Conf. Proc.*, vol. 931, no. 2007, pp. 507–511, 2007.

[58] B. Liu *et al.*, "352nm ultraviolet emission from high-quality crystalline AlN whiskers," *Nanotechnology*, vol. 21, no. 7, 2010.

[59] M. Dabrowska-Szata, "Analysis of RHEED pattern from semiconductor surfaces," *Mater. Chem. Phys.*, vol. 81, no. 2–3, pp. 257–259, 2003.

[60] DoITPoMS (university of cambridge), "Indexing Electron Diffraction Patterns," *university of Cambridge*, 2007. [Online]. Available: https://www.doitpoms.ac.uk/tlplib/diffraction-patterns/index.php. [Accessed: 02-Mar-2021].

[61] M. T. Otten, "HighAngle annular darkfield imaging on a tem/stem system," *J. Electron Microsc. Tech.*, vol. 17, no. 2, pp. 221–230, 1991.

[62] E. (univesity of G. A. Robin *et al.*, "Quantification of dopants in nanomaterials by SEM/EDS," *Eur. Microsc. Congr. 2016 Proc.*, 2016.

[63] T. M. Al Tahtamouni, X. Du, J. Li, J. Lin, and H. Jiang, "Erbium-doped a-plane GaN epilayers synthesized by metal-organic chemical vapor deposition," *Opt. Mater. Express*, vol. 5, no. 2, p. 274, 2015.